arXiv:astro-ph/0301075v1 6 Jan 2003

Gas Kinematics of Three Hickson Compact Groups: The Data [1]

H. Plana [1], P. Amram [2], C. Mendes de Oliveira [3], C. Balkowski [4], J. Boulesteix [2]

ABSTRACT

We present Fabry Perot observations of three Hickson Compact Groups, HCG 88, HCG 89 and HCG 100. We detect ionized gas in 15 group members, three of which were previously uncatalogued objects, two in HCG 89 and one in HCG 100. We were able to derive 2D velocity, monochromatic and continuum maps and rotation curves for a total of 12 giant late-type galaxies and two dwarf galaxies. Even with this small sample of three groups, we can clearly see a trend of kinematic evolution and the different evolutionary stages of the groups. The members of HCG 88 show almost no signs of previous or current interactions, while HCG 100 contains at least two merging and one strongly-interacting galaxies. HCG 89 shows members with signs of interactions and galaxies with normal kinematics. We therefore classify HCG 88, HCG 89 and HCG 100 respectively as an unevolved group, a mildly interacting group and a system in the final stage of evolution.

Subject headings: Galaxies: individual (NGC 6978, NGC 6977, NGC 6976, NGC 6975, NGC 7803)— galaxies: kinematics and dynamics — galaxies: interactions — galaxies: ISM — galaxies: intergalactic medium — instrumentation: interferometers

1. Introduction

Hickson Compact Groups (Hickson 1982, referred hereafter as HCGs) are collections of three to seven galaxies inside a three-magnitude interval, where the members have a projected separation of the order of the galaxy diameter. The original photometric selection criteria found spectroscopic confirmation for 92% of the group candidates (Hickson et al. 1989). With a low velocity dispersion ($\sim 200\ km\ s^{-1}$) and a high galaxy density, Hickson Compact Groups are privileged laboratories to study different stages of interactions, from violent interacting systems to systems with no apparent signs of interaction.

We began in 1995 an observing program using a Fabry-Perot instrument to obtain 2D-velocity maps of Hickson compact group galaxies with the aim of investigating the influence of the dense environment on the kinematics and dynamics of their galaxy members. Such a study is the extension of a previous effort in the same lines, in order to determine the influence of the dense environment of galaxy clusters (Amram et al. 1992, 1993, 1994, 1995, 1996). We first looked at a few particularly interesting groups in detail, in order to understand the evolution of galaxies in such dense environment. The groups already studied were HCG 16 (Mendes de Oliveira et al. 1998), HCG 90 (Plana et al. 1998), HCG 18 (Plana et al. 2000), HCG 92 (The Stefan's Quintet, Plana et al. 1999, Mendes de Oliveira et al. 2001) and HCG 79 (The Seyfert Sextet, Plana et al. 2002). These studies revealed that there are large differences in the kinematic behavior of these systems, between galaxy to galaxy within a group and between one group to

[1]Observatorio Nacional MCT, Rua General Jose Cristino 77, São Christóvão CEP: 20921-400, Rio de Janeiro, RJ, Brazil

[2]Laboratoire d'Astrophysique de Marseille, Observatoire de Marseille, 2 Place Le Verrier, 13248 Marseille Cedex 04 France

[3]Universidade de São Paulo Instituto de Astronomia, Geofísica e Ciências Atmosféricas, Departamento de Astronomia, Rua do Matão 1226 - Cidade Universitária 05508-900 São Paulo SP - Brazil

[4]Observatoire de Paris, GEPI and FRE 2459, CNRS and Université Paris 7, 5 Place Jules Janssen, F-92195 Meudon Cedex, France

[1]Based on observations collected at the European Southern Observatory, La Silla, Chile and at the Canada-France-Hawaii Observatory, Hawaii, USA

the other. Combining the kinematics of the galaxies with other data from the literature we were able to classify the groups in different evolutionary stages, from evolved groups, strongly interacting, to unevolved systems (Mendes de Oliveira & Amram 2000; Amram et al. 2002).

In this paper we present Fabry-Perot data for a set of three Hickson compact groups, HCG 88, HCG 89 and HCG 100. We were able to derive kinematic information for 15 galaxies in these groups.

When available, we also present rotation curves (RCs) from previous studies using long-slit spectroscopy (Rubin et al. 1991, hereafter RHF1991, and Nishiura et al. 2000, hereafter NSOMT2000). A deeper comparison between our results and these previous studies is currently under preparation in a forcoming paper (Mendes de Oliveira et al. 2003 in prep.).

2. Observations

Observations were carried out in two runs at the European Southern Observatory 3.6m telescope (ESO 3.6m) in August 1995 and at the Canada-France-Hawaii 3.6m telescope (CFHT 3.6m) in August 1996. During the run at the ESO 3.6m telescope, the Fabry Perot instrument CIGALE was used. It is composed of a focal reducer (bringing the original f/8 focal ratio of the Cassegrain focus to f/2), a scanning Fabry-Perot and an Image Photon Counting System (IPCS). The IPCS with a time sampling of 1/50 second and zero readout noise makes it possible to scan the interferometer rapidly (typically 5 seconds per channel), avoiding sky transparency, air-mass and seeing variation problems during the exposures.

At the CFHT 3.6m, the multi-object spectrograph focal reducer (MOS) in the Fabry-Perot mode was used, attached to the f/8 Cassegrain focus. The CCD was a STIS 2 detector, 2048 × 2048 pixels with a read-out noise of 9.3 e^- and a pixel size on the sky of 0.86" after 2x2 binning.

Tables 1 and 2 contain the journal of observations and observational characteristics for both runs. Reduction of the data cubes were performed using the CIGALE/ADHOC software (Boulesteix 1999). The data reduction procedure has been extensively described in (Amram et al. 1992) and references therein.

Wavelength calibration was obtained by scanning the narrow Ne 6599 Å line under the same conditions as the observations. Velocities measured relative to the systemic velocity are very accurate, with an error of a fraction of a channel width (< 3 km s^{-1}) over the whole field.

Subtraction of bias, flat fielding of the data and cosmic-ray removal have been performed for each image of the data cube for the CFHT observations. To minimize seeing variation, each scan image was smoothed with a gaussian function of full-width at half maximum equal to the worse-seeing data of the data cube. Transparency and sky foreground fluctuations have also been corrected using field star fluxes and galaxy-free windows for the CFHT observations.

The signal measured along the scanning sequence was separated into two parts: (1) an almost constant level produced by the continuum light in a narrow passband around Hα (continuum map), and (2) a varying part produced by the Hα line (Hα integrated flux map). The continuum level was taken to be the mean of the three faintest channels, to avoid channel noise effects. The Hα integrated flux map was obtained by integrating the monochromatic profile in each pixel. The velocity sampling was 11 $km\ s^{-1}$ at CFHT and 16 $km\ s^{-1}$ at ESO. Profiles were spatially binned to 3×3 or 5×5 pixels in the outer parts, in order to increase the signal-to-noise ratio. Strong OH night sky lines passing through the filters were subtracted by determining the level of emission from extended regions away from the galaxies (Laval et al. 1987).

The different kinematical parameters have been determined as followed. The position angle (PA) of the kinematical major axis has been determined from the velocity field (VF) doing the average of PA estimation at a given radius from the center . The inclination of the VF has been determined using the method described by Amram et al. (1996), consisting of choosing the inclination minimizing the scattering of velocities at determined radius and at different angles from the axis. The kinematical center also has been determined in order to get the most symmetrical rotation curve (RC) when both sides of the velocity plot are folded. Morphological center corresponds to the maximum of the Hα continuum emission. Systemic velocities have been determined using both

the velocity field and the symmetrization of the RC (see last column of Table 4).

3. Description of the individual groups

In this section, we describe the main characteristics of each individual galaxy observed. Table 3 summarizes the general properties of the galaxies and Table 4 gives the different galaxy parameters we derived from the continuum, monochromatic and velocity maps. In Figures 1 to 17, we show the different maps (continuum, monochromatic, velocity), the different rotation curves (RCs) for each group member and, when available, comparison with other authors' data. Group Distances have been derived using the method described in Paturel et al. (1997): the mean group redshifts come from Palombo et al. (1993) and have been corrected to the centroid of the Local Group and for infall of the Local Group towards Virgo using an infall velocity of 170 $km\ s^{-1}$. The distance has been computed using a Hubble constant 75 $km\ s^{-1}\ Mpc^{-1}$. We found D = 80.6 Mpc for HCG 88, D = 119 Mpc for HCG 89 and D = 71.8 Mpc for HCG 100.

3.1. HCG 88

Hickson (1993) described this group as a relatively loose quartet of spiral galaxies with a very small velocity dispersion (27 $km\ s^{-1}$). Ribeiro et al. (1998) detects a set of six galaxies at V = 6074 $km\ s^{-1}$ in the group region and a velocity dispersion of 72 $km\ s^{-1}$. HCG 88a and b are infrared sources, emitting at 60 and 100 μm (IRAS, Allam et al. (1996)) and HCG 88a and HCG 88d are weak radio sources (Menon 1995). Weak CO emission has been detected for HCG 88a (the intensity of the CO line is 1.75 $K\ km\ s^{-1}$, as given by Boselli et al. (1996) and 1.12 $K\ km\ s^{-1}$, given by Léon et al. (1998). HCG 88a shows a weak star formation efficiency (0.22 $L_\odot/M_\odot$) in comparison with the mean SFE of Léon et al. (1998)'s sample (0.39). Verdes-Montenegro et al. (2001) reported a H I deficiency for the whole group of $Def_{H\,I}$ = 0.27, but individual galaxies show a rather large spread in the H I deficiency from 0.92 for HCG 88a to -0.11 for HCG 88c. Ponman et al. (1996) gave an upper limit for the X-ray luminosity of the group of 42.18 erg s^{-1} (using the H_o = 50 $km\ s^{-1}\ Mpc^{-1}$). Ribeiro et al. (1998) found that this group is formed by a total of six members and reinforce the idea that HCG 88 is an isolated compact group.

We present continuum and monochromatic maps and velocity fields for all four group members. Shimada et al. (2000) detected only [N II]-line emission and did not detect Hα-line emission in the nucleus of HCG 88a. They classified this galaxy as an AGN. We detect Hα emission throughout the disk of HCG 88a, in a clumpy distribution. The velocity field of HCG 88a is fairly regular but slightly twisted around the kinematic major axis. RHF1991 and NSOMT2000 published RCs for HCG 88a, obtained from long-slit spectroscopy, along the major axis of the galaxy. In Fig. 3a we compare the three curves (ours, RHF1991 and NSOMT2000). The inclination used to derive these curves is very similar (65, 68 and 64 degrees, respectively). The RC derived by RHF1991 matches that derived by us better than NSOMT2000 does. Nevertheless, even in that case the agreement is not satisfactory. The RC derived in this study is symmetric, i.e. both sides of the curve match, which is not observed in the RC derived by RHF1991. Indeed, the latter displays a flat approaching side and a rising receding side, while in the present paper we find that both sides are rising [6]. The disagreement between both sides of RHF1991's RC is probably due to a bad choice of the kinematic center of rotation, as it can be suspected from the strong disagreement between both sides of their RC around the center, within 5 arcsec. The RC derived by NSOMT2000 does not agree with those derived by us and by RHF1991. Moreover, they derive an RC out to 16 arcsec only, while RHF1991 and this paper present RCs which extend out to 32 arcsec (12.5 kpc).

The SBb galaxy HCG 88b presents a very clumpy monochromatic map, with a strong asymmetric emission in an arm-like feature in the north-eastern side and a less strong emission region in the southern region. In contrast, on the north-western side of the galaxy, almost no emission can

[6] In table 7 of RHF1991, as well as in their Fig. 1, it is indicated that positive radial distances refer to the tabulated position angles. Nevertheless, the two galaxies of this group presented in their paper display an RC reversed with respect to what we derived. We assume that this is a mistake, and reverse the sign of their data, to compare them to ours.

be seen. Due to the presence of a bar in this galaxy (SBb), the continuum image shows an asymmetric and irregular shape, rotating from 34^o within 10 arcsec to 160^o at a radius of 30 arcsec. At large radius (50 arsec) the galaxy is rather round. The velocity field shows a large scale twist and a clear signature of a bar in the inner regions. The RC derived in this study is completely asymmetric, with a total extension of 40 arcsec (15.6 kpc). Approaching and receding sides match well in the inner 5 arcsec and they disagree farther out. The maximum discrepancy happens at a radius of 20 arcsec (7.8 kpc), where the approaching side has velocities 80 $km\ s^{-1}$ lower than that in the receding side. Fig. 3b shows our data together with that from NSOMT2000. The RC obtained by NSOMT2000 is plotted with a PA = 31^o, which is orthogonal with respect to the PA = 160^o we derived for the major axis of this galaxy. This obviously leads to very different results, which cannot be directly compared. However, even if we use NSOMT2000's kinematic parameters (inclination and PA) and simulate a long slit in our data, we cannot reproduce their RC, specially for the receding side (Mendes de Oliveira et al.2003, in prep.).

HCG 88c shows a rather symmetric gas distribution of what could be a three-arm system. The brightest $H\alpha$ knot coincides with the continuum center. The continuum image shows an arm-like structure on the southeastern side of the galaxy and an asymmetric feature (the eastern isophotes are stretched as compared to the western isophotes). The velocity field is regular even if a twist can be seen (less strong than for HCG 88b). The RC of HCG 88c, slightly rising from 4 arcsec (1.6 kpc) to 25 arcsec (9.8 kpc), displays a good match between the receding and approaching sides (Fig. 4b). The RC reaches 35 arcsec (13.7 kpc, 0.9 R_{25}) at a velocity of 120 $km\ s^{-1}$. Fig. 6a plots the RC derived in this study together with those derived by NSOMT2000 and RHF1991. NSOMT2000 seems to have used a wrong PA for the major axis (31^o instead of 160^o used by RHF1991).

The RC derived by RHF1991 extends to 20" (7.8 kpc) and agrees quite well to our except the part after -20" on the receding side and the two extreme points respectively at 24" (9.5 kpc) and at 28" (11.8 kpc) on the approaching side (see Fig. 6a).

The edge-on Sc galaxy HCG 88d shows an asymmetric continuum image with respect to the line of nodes, due to a dust lane. The monochromatic image shows a clumpy structure exhibiting five rather strong Hα knots. The velocity field is regular. The RC derived in this study is symmetric and rising till 60 arcsec (23.4 kpc) for a rotational velocity of 260 $km\ s^{-1}$ (Fig. 5b). The solid-body shape is probably a result of absorption effects due to the high-inclination of the galaxy (85^o). The agreement between NSOMT2000 and our data (Fig. 6b) is acceptable for the overall shape of the curves but not in the details, specially between 10 and 20 arcsec, where NSOMT2000 find a flat RC. Moreover, the RCs derived by NSOMT2000 ends around a radius of 21 arcsec in the in the southwestern region and of 26 arcsec in the northeastern part. NSOMT2000 noted that HCG 88b and 88d have lower rotational velocities than field spiral galaxies with similar Hubble types and luminosities; this is obviously due to the small extension of the RC they derived.

3.2. HCG 89

This group is one of the most distant ones in our sample (119 Mpc). It is formed by four spiral galaxies. Allam et al. (1996) gave possible detections of galaxies HCG 89c and HCG 89d and upper limits of HCG 89a and 89b, at 60 μm ($<$ 0.18 Jy for HCG 89a, $<$ 0.16 Jy for HCG 89b and a value of 0.31 Jy for HGC 89 cd, together). CO emission has only been detected for HCG 89c (Léon et al. 1998) with an intensity of 0.56 $K\ km\ s^{-1}$, which is the lowest value for Léon et al. (1998)'s sample. Verdes-Montenegro et al. (2001) showed that this group exhibits almost no H I deficit ($Def_{H\,I} = 0.04$). Ponman et al. (1996) listed an upper limit for the X-ray luminosity ($< 42.30\ erg\ s^{-1}$, using $H_o = 50\ km\ s^{-1}$ Mpc^{-1}). Shimada et al. (2000) reported nuclear emission in several lines (Hα, [NII]6584 Å and [NII]6548 Å) for HCG 89a and classified it as having an H I activity type.

We derived maps for the four members. We also found a new (non-catalogued) member near HCG 89a. The monochromatic map and continuum image of HCG 89a show that the galaxy has an arm-like structure with almost no emission in its center. A very bright knot can be seen on the southwestern side of the disk of HCG 89a. This

was noted by RHF1991, who suspected that this knot was a tidal dwarf candidate. The brightest part of the Hα knot is very round and a velocity gradient of $\sim$ 60 $km\ s^{-1}$ can be measured from one side to the other. This very bright giant H II region will perhaps become a tidal dwarf galaxy. However, what we can say is that, in the present, its velocity gradient matches perfectly the grand design velocity field of the galaxy.

At about 37 arcsec (21.3 kpc) south of HCG 89a, a bright emission region is visible in the Hα monochromatic map, we called HCG 89x on Fig. 7a. At very low intensity level (not shown here), our continuum image shows that this isolated region is in fact weakly linked (by a stellar bridge) to the main body of HCG 89a. We do not know the absolute velocity of this object since we have no absolute measurement of it, but only relative velocities subject to a shift of the free spectral range of the interferometer (265 $km\ s^{-1}$). The range of possible velocities is provided by the limits of the interference filter (computed at 20 per cent of the maximum transmission), i.e. in a range between 7870 and 10145 $km\ s^{-1}$. Eight values for the systemic velocity of this region are possible: $9190 \pm n \times 265\ km\ s^{-1}$ where $1 < n < 4$). This giant Hα knot, which has a size around 7 arcsec (4 kpc), shows a clear velocity gradient of 84 $km\ s^{-1}$ ($\pm$ 42 $km\ s^{-1}$) decoupled from the velocity field of the main body of the galaxy. This object is not in counter-rotation with respect to the main body (the position of its major axis is 80^o while the one of the main body is 54^o). Moreover, it does not show any geometrical or velocity continuity with the main velocity field. A fairly regular RC has been plotted for this object (Fig. 11b). Both sides agree and reach a maximum rotational velocity around 70 $km\ s^{-1}$ (for an inclination of 50 ± 6^o). This provides a mass which is high enough for the galaxy to be self-graviting. In conclusion, the emission-line system south of galaxy HCG 89a is, in fact, an excellent tidal dwarf candidate.

The kinematic and stellar major-axis position angles of HCG 89a differ by 10^o (see table 4). The velocity field of HCG 89a shows no major twisted isovelocities at large radii, which is confirmed by the symmetric RC for radii larger than 8 arcsec (4.6 kpc). The southeastern bright extension of the velocity field is described below. In the inner region of the galaxy, a very steep velocity gradient is observed to the northeast (receding side), up to 4 arcsec (2.3 kpc, 170 $km\ s^{-1}$), followed by a decrease of 40 $km\ s^{-1}$ to 8 arcsec (4.6 kpc, 130 $km\ s^{-1}$). Farther out, the two sides of the galaxy match. Note that this high-velocity spot does not present any morphological counter part neither in the Hα map nor in the continuum image. In the northwestern side of the galaxy, the velocities rise regularly. This non-bulgy galaxy is not classified as a barred galaxy. In fact, the asymmetric signature of the velocity field could not be due to a bar perturbation since that would give rise to a symmetric feature. The RC of HCG 89a extends up to 30 arcsec (17.3 kpc) for a velocity of 215 $km\ s^{-1}$. RHF1991 and NSOMT2000 published RCs for this galaxy, which can be compared to that derived here. The RC derived by RHF1991 is symmetric and reaches 25 arcsec (14.4 kpc), where the receding and approaching sides match well except for the high velocity spot and the depression discussed before. The shape of both RCs is quite similar (we also can notice the presence of the high velocity region at -5") except for the approaching part when, our RC decreases and their has a flat shape. The main difference between our data and their (Fig. 9a), comes from the velocity amplitude (210 $km\ s^{-1}$ and 130 $km\ s^{-1}$ respectively). This difference is due to the kinematic inclination we deduced from the velocity field (45^o) and the inclination deduced from the photometry by RHF1991 (60^o). Indeed, the velocity dispersion observed at each radius for different azimuthal angles reaches a minimum for an inclination of 45 ± 5^o, (see Amram et al. (1996) for more details on the method we used to determine the inclination). On the other hand, the morphological inclination is indeed the value used by RHF1991 (60^o), if one excludes the southeastern knot discussed above. As this knot is visible in the continuum image and as we argued that this knot belongs to the main body of the galaxy, there is no reason to exclude it to determine the inclination of the galaxy. Including this knot, the morphological inclination becomes compatible with the kinematic one (45 ± 5^o). The RC determined by NSOMT2000 is more irregular than that of RHF1991 and ours, emphasizing the high velocity region. In addition, it does not reach as far out as the other RC's do (only out to 20"). The velocity amplitudes derived

by NSOMT2000 agree better with ours because the inclination adopted (51^o) is more similar to the inclination derived by us.

The monochromatic and continuum images of HCG 89b show well a spiral structure. In addition, the monochromatic image shows large emission complexes, the largest being a region to the northeast of the galaxy. As for HCG 89a, weak emission is visible in its center. The gas and stellar major-axis position angles of this galaxy differ by 10^o. HCG 89b was morphologically classified as a barred galaxy, an SBc (Hickson 1993) and, indeed, a weak bar signature can be seen through the tilt of its central isovelocities. The regular RC shows a continuous increase of the rotational velocity up to 130 $km\ s^{-1}$ at a radius of 6 arcsec (3.5 kpc), after which a plateau is reached. After 16 arcsec (9.2 kpc), the trend of the receding side decreases, while the approaching side slowly rises, out to a radius of 25 arcsec (14.4 kpc), up to a velocity of 175 $km\ s^{-1}$. The RC derived by RHF1991's shows a solid body rotation continuously rising from -10 arcsec to 22 arcsec. The main difference between the RC derived by RHF1991 and that derived by us (Fig. 9b) comes from the different values of our derived inclination and theirs (49^o and 63^o). Even if we use our continuum map to derive a photometric inclination (which is presumably what they used), the value we find is 56^o (see table 4), still lower than the value of inclination used by RHF1991 to derive the RC of HCG 89b. Simulating a long slit on our VF and using RHF1991's parameters, we can nevertheless derive a rotation curve matching better RHF1991 curve (Mendes de Oliveira et al. 2003, in prep.).

A bright Hα emission region is seen at about 38" to the southwest of the center of HCG 89b. Its size is approximately 9 arcsec (5.2 kpc). Contrary to the giant Hα knot seen close to HCG 89a, this region presents a very small velocity gradient, of the order of its velocity dispersion (15 $km\ s^{-1}$). We, therefore, cannot assess if this objet is a tidal dwarf candidate or not. In Fig.7a, this object is labelled HCG 89x.

HCG 89c and HCG 89d are separated by only 32" and were, therefore, imaged in one single exposure. HCG 89c is one and a half times larger than HCG 89d (maximum radius of 24 and 15 arcsec respectively) and it has a maximum rotational velocity almost three times as high as that for HCG 89d (180 and 70 $km\ s^{-1}$ respectively). In both cases, the agreement between both sides of the RC is good in the central regions but diverge somewhat in the external regions. Both galaxies have a clumpy monochromatic map, but HCG 89d is brighter than HCG 89c in Hα, showing clearly three bright knots in emission. The velocity field of HCG 89c is regular in the inner part but the external isovelocities are peculiar. The velocity field of HCG 89d presents an U-shape twist around the major axis which can explain the peculiarity of the RC. Moreover, HCG 89d shows an extension to the south toward the direction of HCG 89c. This extension could maybe be explained by an interaction between the two galaxies even if the velocity difference is rather large between the extension of HCG 89d (8740 $km\ s^{-1}$) and the northern part of the velocity field of HCG 89c (8920 $km\ s^{-1}$).

3.3. HCG 100

This quartet, formed by four late-type galaxies, shows a bright central Sb galaxy with strong infra-red emission. Allam et al. (1996) give IRAS fluxes for HCG 100a ($F_{60}\mu$m = 1.75 Jy, $F_{100}\mu$m = 4.33 Jy) and upper limits for the remaining galaxies in the group ($F_{60}\mu$m < 0.17 Jy, $F_{100}\mu$m < 0.71 Jy). Only an upper limit has been determined for the X-Ray luminosity of this group, by Ponman et al. (1996). Verdes-Montenegro et al. (2001) give an H I deficit $Def_{HI} = 0.5$ for the whole group, higher than the mean value for their sample. Léon et al. (1998) have detected CO gas for HCG 100a only, and derived an SFE of 0.72 L$\odot$/M$\odot$, a value above the mean for their sample. Although HCG 100d has no measured redshift, we know it is a member of the group because we were able to detect gas emission from it. It has, therefore, a velocity within the velocity range of our inference filter (within 265 $km\ s^{-1}$). We also detected a new point-like source (not previously catalogued) east of HCG 100b. We could derive maps for all four members and for the new object as well.

The monochromatic image of HCG 100a shows bipolar emission regions but no emission is seen at the position of the continuum center, as mentioned by Vilchez et al. (1998). The general morphology of the monochromatic map derived by Vilchez et al. (1998) is similar to that derived by us. Their map reaches an extension of 31", if we include the emission spot to the east of their map. This spot

can also be seen on our map, at the same location and distance from the center (a radius of $\sim$ 19" along the major axis). Our continuum map shows a regular distribution of light, with an elliptical shape, and without any detected spiral pattern. The velocity map shows that the extension to the east does not have a velocity gradient but, instead, it corresponds to a single isovelocity. We note that there is a variation of the position angle of the major axis along the radius of the galaxy. We also note three isovelocities which are inconsistent with the rest of the velocity field, located northwest and southeast of the galaxy. The RC for H100a is not symmetric, showing a flat part beyond a radius of 8 arcsec (2.8 kpc) on the receding side and a constantly rising velocity in the approaching side. We compare the RC with that derived by RHF1991 (Fig. 16a). They used an inclination of 60^o and a PA = 85^o, compared to 50^o and 78^o for our data. The agreement between the two RCs is good for the receding side but for the approaching side the velocity amplitudes given by RFH1991 are larger than those derived by us.

HCG 100b has been classified as an Sm galaxy by (Hickson 1993), but our data (and the velocity field in particular) suggests that this object is more likely irregular. The extension of the monochromatic image of this galaxy is $\sim$ 22", comparable to what was derived by Vilchez et al. (1998). We can clearly see the central emission and the tail-like feature in the southeast direction. We also note, by comparing the monochromatic and continuum maps, that there is a difference of 25^o degrees between the PA of the two major axes. The velocity field appears to be disturbed, with a strong variation of the position angle along the radius. In addition, some isovelosities are inconsistent with those measured over the whole map. The RC of HCG 100b is obviously asymmetric: there is no match between the two sides of the galaxy. In fact, the RC is so peculiar that it does not have an approaching side. The rotation of this object is not consistent with a disk-like rotator.

HCG 100c is a late-type barred spiral galaxy. The monochromatic map shows strong central emission with an extension out to a radius of 35". Vilchez et al. (1998) show an Hα image of the central part of the galaxy only. The PA of the major axis obtained in the continuum map is slightly different from the monochromatic map (stellar and kinematic axes differ by 20^o). The velocity map clearly shows the presence of the bar, with the central 5425 $km\ s^{-1}$ isovelocity. The velocity field also shows the strong variation of the major axis along the radius and presents inconsistent isovelocities to the northeast. The RC of HCG 100c shows pretty good agreement between both sides out to a radius of 13 arcsec (4.5 kpc). Further out, the receding side continues to rise out to 14 arcsec (4.9 kpc) and then reach a plateau. The approaching side has dropping velocities for radii between 13 arcsec to 20 arcsec (7 kpc). This drop corresponds to the inconsistent isovelocities to the northeast of the velocity field. We compare the RC derived in this study with that derived by RFH1991 (Fig. 16b). There is good agreement only in the center.

HCG 100d is a late-type edge-on spiral galaxy. No redshift information is available for this object but, due to the narrow FHWM of our interference filter (17 Å = 777 $km\ s^{-1}$), the probability for this object to be part of the group is high. The monochromatic image of the galaxy shows a clumpy structure, consistent with the image produced by Vilchez et al. (1998). The continuum map is regular, but with a knot to the northeast. The knot corresponds to an excess emission on the monochromatic map. The velocity field if fairly regular but also shows a variation of the isovelocities along the radius. The RC of HCG 100d is continuously rising, both sides agree well within 8 arcsec (2.8 kpc) and further out the discrepancy between both sides increases with radius. The velocity amplitudes reach 240 $km\ s^{-1}$ and 170 $km\ s^{-1}$ for the approaching and receding sides respectively at a radius of 30 arcsec (10.4 kpc).

HCG 100x is an extragalactic emission object located 30" east of HCG 100b. We did not find any mention of this object in the literature. This object has an Hα extension of 20" and a very compact and intense nucleus of 5" radius. Line emission and continuum emission are concentrated in the nucleus but we observed a shift of 2 arcsec between both maxima. The velocity map is not axisymmetric, as can be seen also in the RC. The approaching and receding sides of the RC disagree completely.

4. General discussion and Conclusions

4.1. A census of the interaction-related properties of the galaxies

One of the main reasons why it is important to have the full kinematic information for each compact-group member is to have some insight about the possible interaction history of the galaxy. Mendes de Oliveira et al. (1998) described several interaction indicators and listed those present in the galaxies studied by them. Similarly, in Table 5, we list different indicators for all the galaxies studied here. Different interaction scenarios, depending on the strength of the encounter and the morphological types of the interacting systems, will leave different signatures on the velocity fields of the galaxies. As discussed in Mendes de Oliveira et al. (1998), indicators like *highly disturbed velocity field, double nuclei and double kinematic gas component* are used to show strong evidences for merger. Other indicators such as *warping, stellar and gas major axis misalignment, tidal tail, high IR luminosity and central activity* are used to show indications of collisions which do not lead to merging.

4.2. The interaction history of each galaxy

The data presented in this paper support the existence of regular gaseous rotating disks in the centers of all studied galaxies, except for HCG 100b. Based on the interaction indicators for each galaxy listed in Table 5 and in the context of the various models of galaxy interactions (Barnes (1989), Barnes & Hernquist (1992, 1996)) we suggest the following histories for the 12 giant galaxies studied here.

Galaxies HCG 88c, HCG 88d and HCG 100d seem to be undisturbed galaxies, with no signs of interaction. However, HCG 88d and HCG 100d may be in unfavorable inclinations to see any signs of interaction in their velocity fields. Although we have small number statistics, this small sample of undisturbed galaxies is composed of the faintest members of their respective groups.

Galaxies HCG 88a, HCG 88b, HCG 89a, HCG 89b, HCG 89c and HCG 89d seem to have suffered mild interaction. HCG 89a has a strong kinematic peculiarity only in its center. HCG 89c has a peculiar velocity field but no other sign of strong interaction. The remaining galaxies show evidence for mild interaction histories.

Galaxies HCG 100a, HCG 100b and HCG 100c are galaxies which show strong interaction. These are all in one single group, suggesting that in this group strong encounters have happened in the past. This group must be, therefore, in an advanced stage of evolution. HCG 100a may have also suffered a major accretion event, given its very peculiar velocity field.

4.3. The evolutionary stage of each group

Based on the description above, our summary for the evolutionary history of the three groups is the following.

HCG 88 does not display many indicators of having suffered interaction and it displays no indicators of merging. HCG 88c and HCG 88d do not show any interaction signature at all. We should note, however, that the RC for HCG 88d is difficult to obtain because of the high inclination of the disk. HCG 88b has the most disturbed velocity field for this group and it has the least regular RC of the four galaxies of the group. However, it cannot be classified as "highly disturbed", as other galaxies in group HCG 100 are. HCG 88a is an active galaxy but there is no evidence in its velocity field, that this galaxy has suffered interactions in the recent past. This is not an unexpected result, since it is well known that although active galaxies often appear to be in interaction, it is not always the case. In conclusion, HCG 88 may be an unevolved group, which has recently formed, with low level of interaction. This is in agreement with the conclusion from the H I kinematic study of this group (Verdes-Montenegro et al. 2001).

The list of Table 5 shows that the galaxies in HCG 89 have more positive indicators than those in HCG 88. HCG 89c seems to have the most disturbed velocity field. HCG 89b, HCG 89c and HCG 89d show mildly disturbed rotation curves. HCG 89a has a large disturbance in its center, perhaps because of the canibalism of a small galaxy, or perhaps due to an interaction with the bright emission blob present in the eastern part of the galaxy. The difference of systemic velocities between HCG 89c and HCG 89d is only 40 $km\ s^{-1}$ and the projected distance is 30 arcsec. It is tempting to say that these two objects may be in

interaction. The velocity field of HCG 89d shows an extension to the south, towards HCG 89c, but the velocity difference between the two galaxies is 180 $km\ s^{-1}$, which is too large for a scenario of gas exchange between the two objects. This distant group does not have a lot of ISM material but HCG 89d clearly shows an excess of warm gas in comparison with HCG 89c. We conclude that this group is in an intermediate evolutionary phase, not as unevolved as HCG 88 but also not as evolved as HCG 100.

HCG 100 shows many signs of interactions. Three of the four giant galaxies of the group have a highly disturbed velocity field and no member has a RC which is completely regular and axisymetric (however we should note that the peculiarity for HCG 100d is small but difficult to detect due to its high inclination). Change of PA of the major axis along the radius is also present for three galaxies in this group. However, no central activity has been found for any group member. The most disturbed group member is HCG 100b. This object may be the product of a merger. In conclusion, HCG 100 is the most evolved group of the three studied here.

H.P. would like to thank the Brazilian PRONEX program, for financial help to attend the conference "Galaxies: The Third Dimension" in Cozumel (Mexico), Dec. 3-7 2001 and the Marseille Observatory Scientific Council for financial help during his stay at the Marseille Observatory in May/June 2002. H.P. also acknowledges the financial support of Brazilian Cnpq under contract 150089/98-8. CMdO acknowledges financial support from PRONEX and FAPESP. The authors thank J.L. Gach for helping during the observations. The NASA/IPAC Extragalactic Database (NED) is operated by the Jet Propulsion Laboratory, California Institute of Technology, under contract with NASA.

REFERENCES

Allam S., Assendorp R., Longo G., Braun M., Richter G. 1996, A&AS, 117, 39

Amram P., Le Coarer E., Marcelin M., Balkowski C., Sullivan W. T. III, Cayatte V. 1992, A&AS, 94, 175

Amram P., Sullivan W., Balkowski C.,Marcelin M., Cayatte V., 1993, ApJ, 403, L59

Amram P., Marcelin M., Balkowski C., Cayatte V., Sullivan W. T. III, Le Coarer E. 1994, A&AS, 103, 5

Amram P., Boulesteix, J., Marcelin M., Balkowski C., Cayatte V., Sullivan W.T.,III, 1995, A&AS, 113, 35

Amram P., Balkowski C., Boulesteix J., Cayatte V., Marcelin M., Sullivan W., 1996, A&A, 310, 737

Amram P., Mendes de Oliveira C., Plana H., Balkowski C., Boulesteix J., Carignan C. 2002, Astrophysics and Space Science, 281, p. 389-392

Barnes J., 1989, Nature, 338, 123

Barnes J., Hernquist L., 1992, Nature, 360, 715

Barnes J., Hernquist L., 1996, ApJ, 471, 115

Boselli A., Mendes de Oliveira C., Balkowski C., Cayatte V., Casoli F. 1996, A&A, 314, 738

Boulesteix J., 1999, User Manual of ADHOCw reduction Package Publication of Observatoire de Marseille, http://www-obs.cnrs-mrs.fr/adhoc

de Carvalho R.R., Ribeiro A.L.B., Zepf S.E. 1994, ApJS 93, 47

Jarvis J. 1986 AJ, 91, 65

Laval A., Boulesteix J., Georgelin Y.P., Georgelin Y.M., Marcelin M. 1987, A&A, 175, 199

Hickson P. 1982, ApJ, 255, 382

Hickson P., Kindl E., Auman J. 1989, ApJS, 70, 687

Hickson P. 1993, ApLetter&Comm 29, 1

Léon S., Combes F., Menon T.K. 1998, A&A, 330 37

Mendes de Oliveira C., Plana H., Amram P., Balkowski C., Boulesteix J. 1998, ApJ, 507, 691

Mendes de Oliveira C., Amram P. 2000, PASP, Small Galaxy Groups: IAU Colloquium 174, ASP Conf. Series, Vol. 209, p60. Ed. Mauri J. Valtonen and Chris Flynn.

Mendes de Oliveira C., Plana H., Amram P., Balkowski C., Bolte M., 2001, AJ, 121,2524

Menon T.K. 1995, MNRAS, 274 845

Nishiura S., Shimada M., Ohyama Y., Murayama T., Taniguchi Y. 2000, AJ, 120, 169 (NSOMT2000)

Palumbo G.G.C., Saracco P., Mendes de Oliveira C., Hickson P., Tornatore V., Baiesi-Pillastrini G.C. 1993, ApJ, 405, 413

Paturel G., Andernach H., Bottinelli L., di Nella H., Durand N., Garnier R., Gouguenheim L., Lanoix P., Marthinet M., Petit C., Rousseau J., Theureau G., Vauglin I. 1997, A&A Supplement series, 124, 109

Pildis R.A., Bregman J.N., Schombert J.M. 1995, AJ, 110, 1498

Plana H., Mendes de Oliveira C., Amram P., Boulesteix J., 1998, AJ, 116, 2123

Plana H., Mendes de Oliveira C., Amram P., Bolte M., Balkowski C., Boulesteix J., 1999, AJ, 516,L69

Plana H., Amram P., Mendes de Oliveira C., Balkowski C., 2000, AJ, 120, 621

Plana H., Sulentic J., Mendes de Oliveira C., Amram P., Balkowski C., Rosado M., 2002, in *Galaxies: the Third Dimension, ASP Conf. Series, Ed. M. Rosado, L. Binette and L. Arias, in press*

Ponman T. J., Bourner P.D.J., Ebeling H., Bohringer H. 1996, MNRAS, 283, 690

Ribeiro A.L.B., de Carvalho R.R., Capelato H.V., Zepf S.E. 1998, ApJ, 487, 72

Rubin V.C., Hunter D.A., Ford W.K.Jr. 1991, ApJS, 76, 153 (RHF1991)

Shimada M., Ohyama Y., Nishiura S., Murayama T., Taniguchi Y. 2000 AJ, 119, 2664

Verdes-Montenegro L., Yun M.S., Williams B.A., Huchtmeier W.K., Del Olmo A., Perea, J. 2001, A&A, 377, 812

Vilchez J.M., Iglesias-Paramo J., 1998, ApJS, 117, 1

Williams B.A.1985, ApJ290, 462

This 2-column preprint was prepared with the AAS LaTeX macros v5.0.

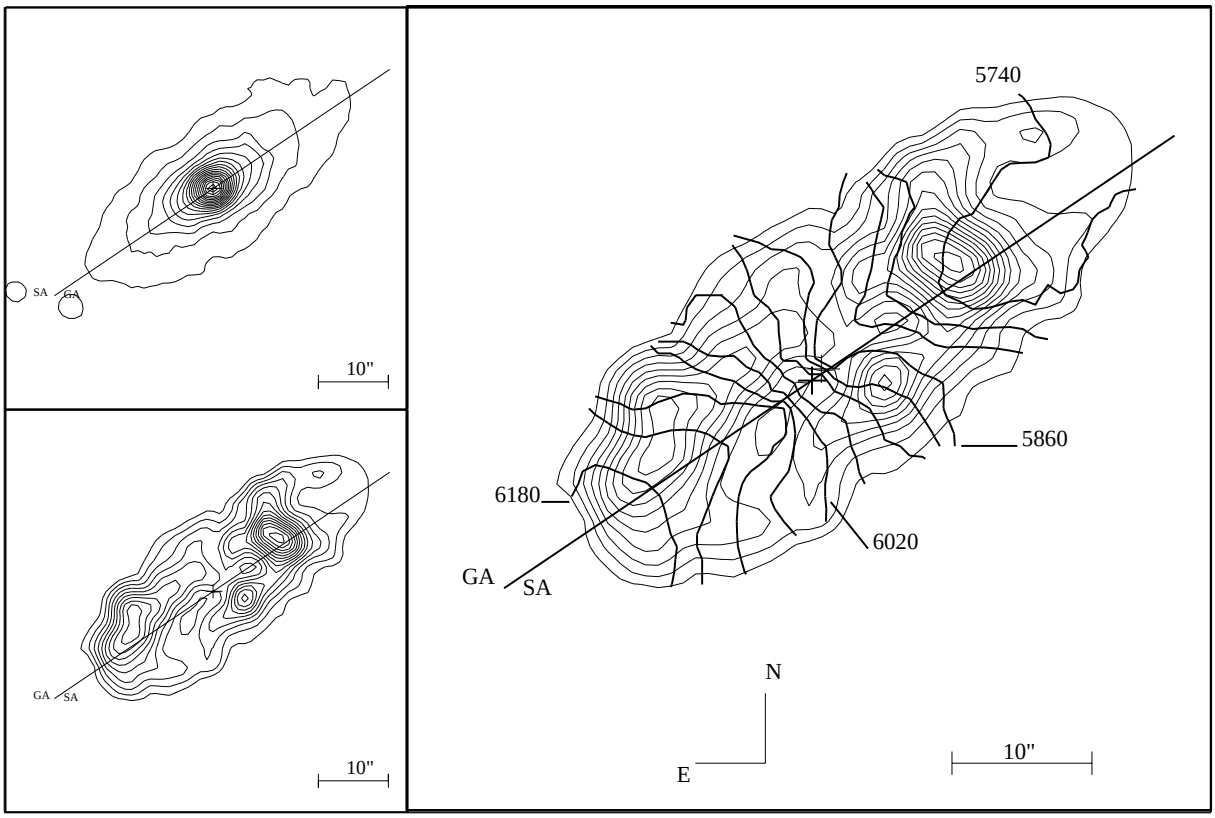

Fig. 1a.— HCG 88a: Upper left panel represents the continuum map with respectively the stellar axis (SA) and the monochromatic map axis (GA). Lower left panel is the monochromatic map. Right panel is the velocity field (in bold) superimposed to the monochromatic map. GA axis represents the major axis of the velocity field, SA axis is the major axis of the continuum map. Bold cross represents the kinematical center.

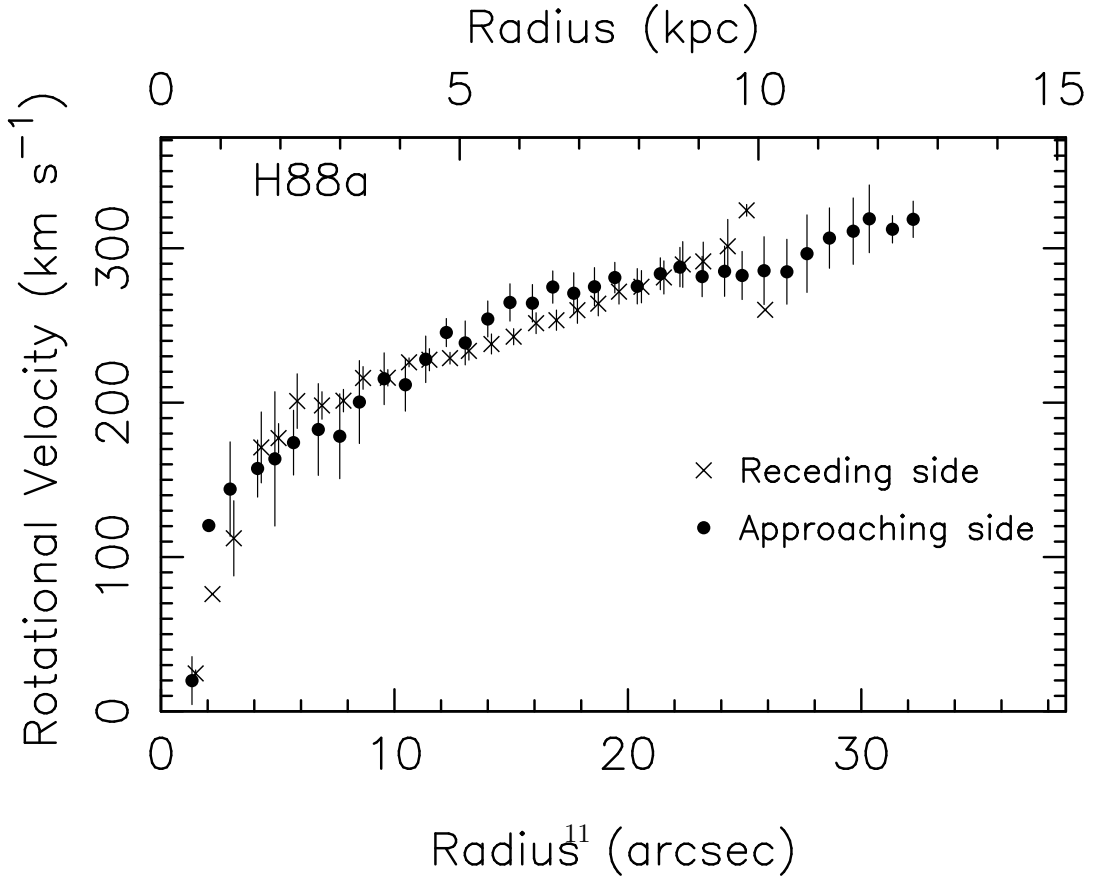

Fig. 1b.— HCG 88a: Rotation curve. Arrow represents the R_{25} isophote from RC3 catalog, when available.

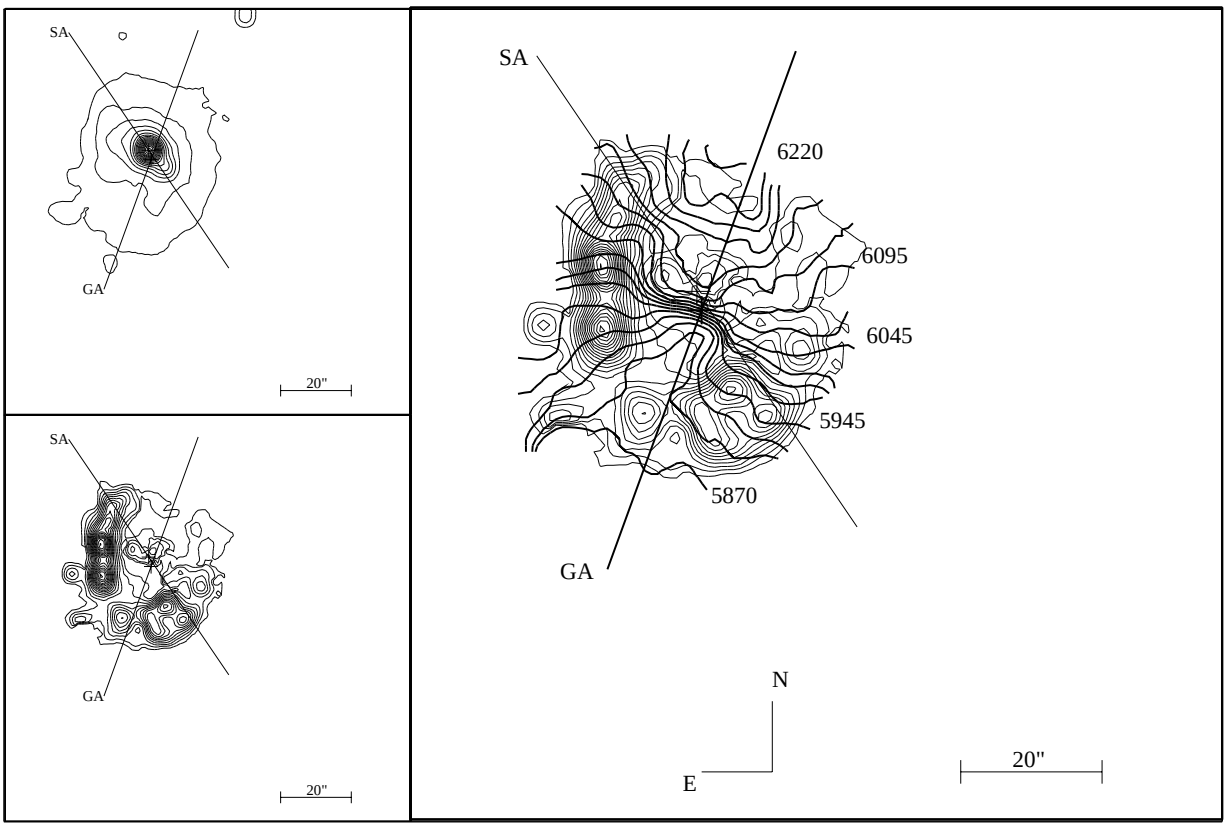

Fig. 2a.— HCG 88b: same as Fig.1a

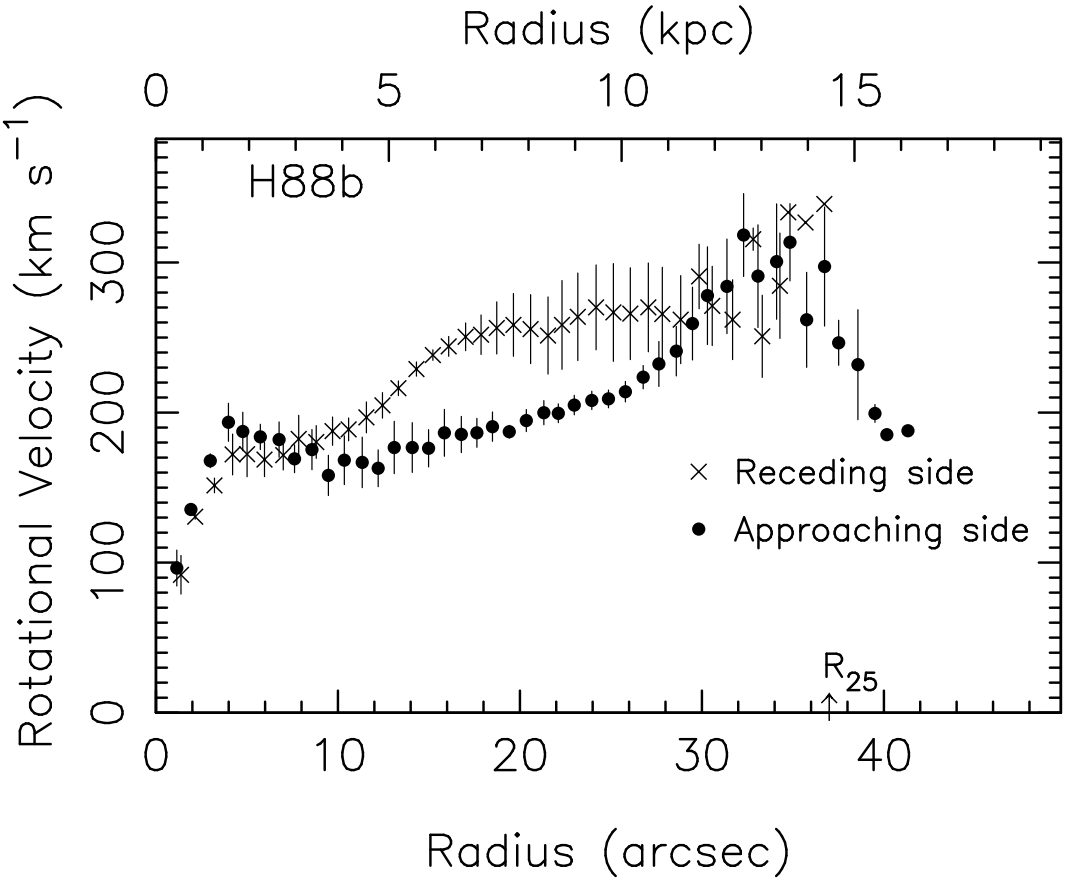

Fig. 2b.— HCG 88b: same as Fig.1b

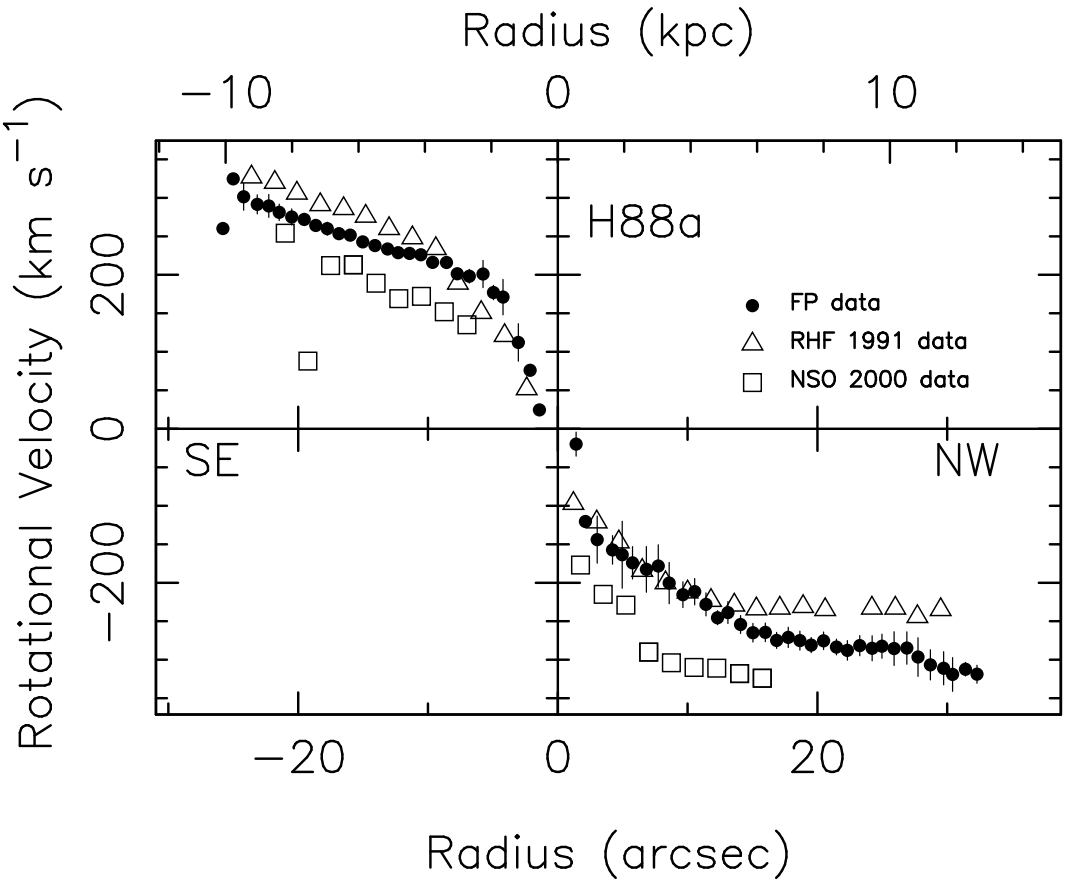

Fig. 3a.— HCG 88a: we are presenting different rotation curves using our data, RHF1991 data and NSOMT2000 data. The kinematical parameters used to plot the rotation curves are, for the inclination, 65^o, 68^o and 64^o respectively and for the position angle of the major axis, 128^o, 127^o and 132^o respectively.

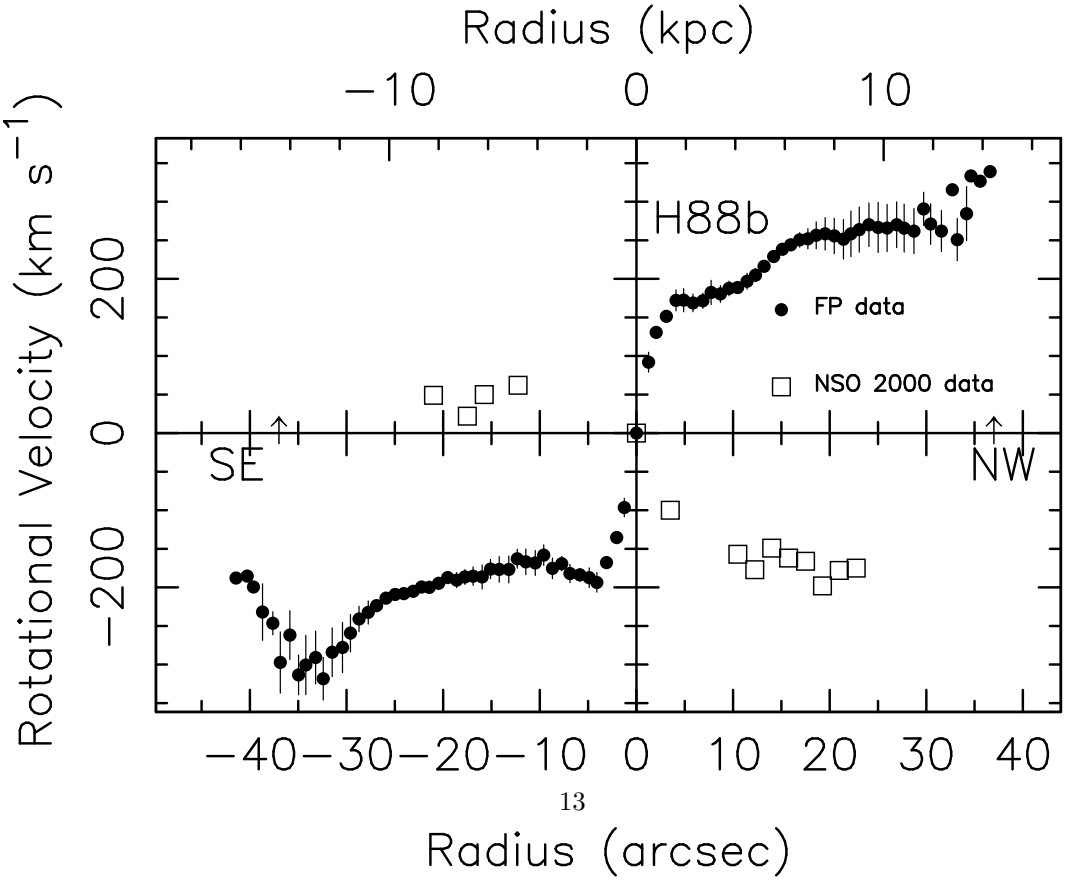

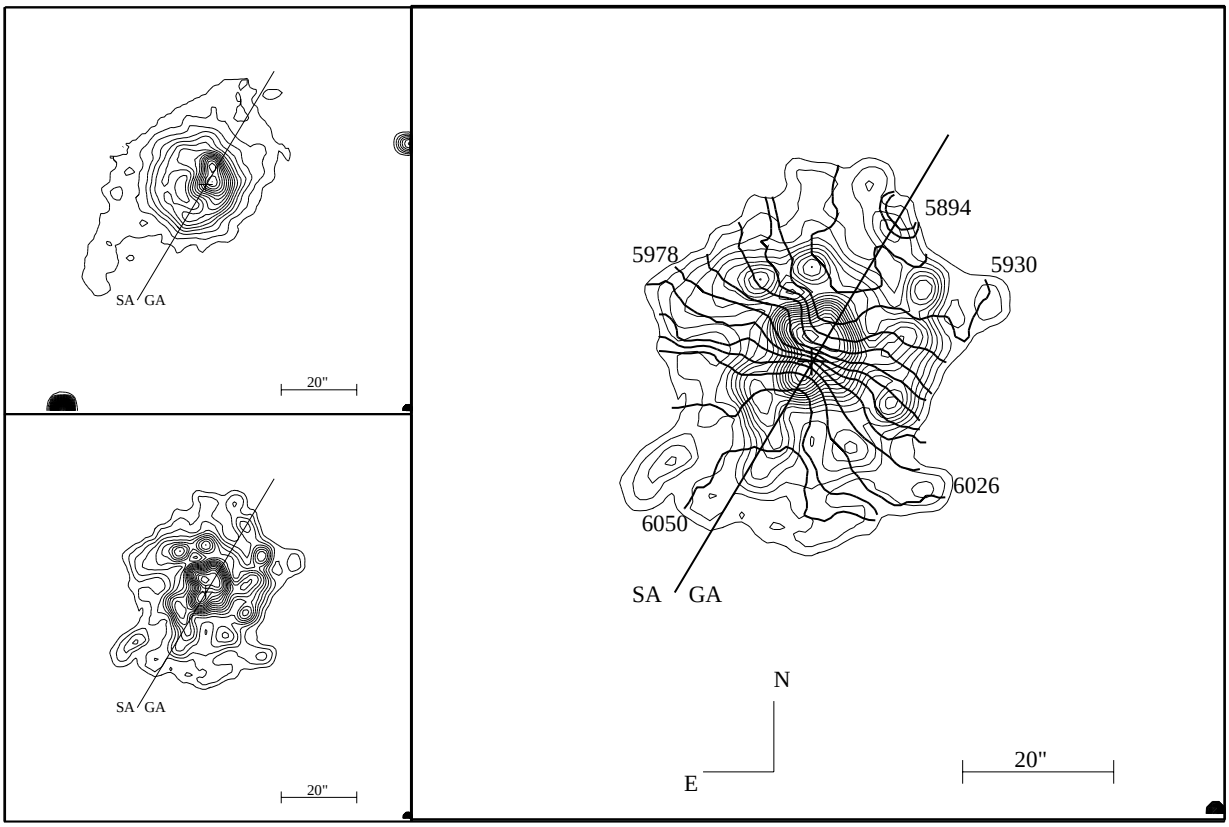

Fig. 4a.— HCG 88c: same as Fig.1a

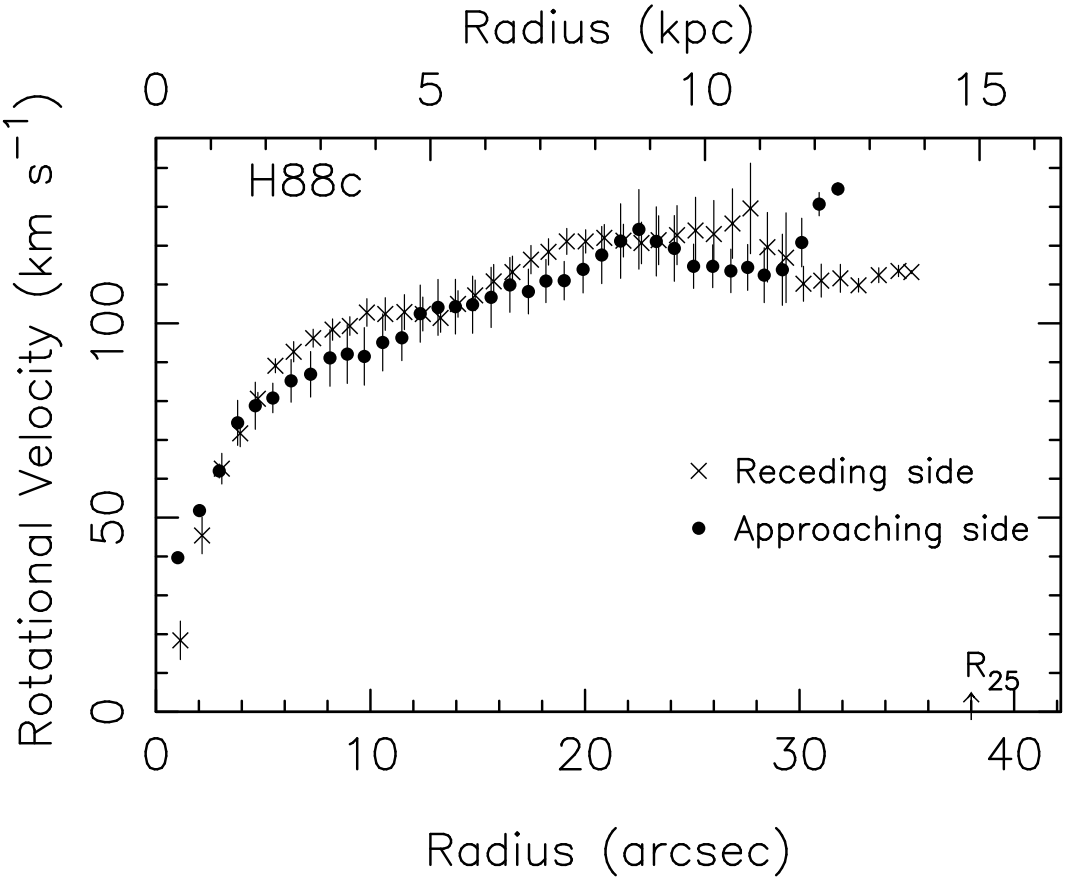

Fig. 4b.— HCG 88c: same as Fig.1b

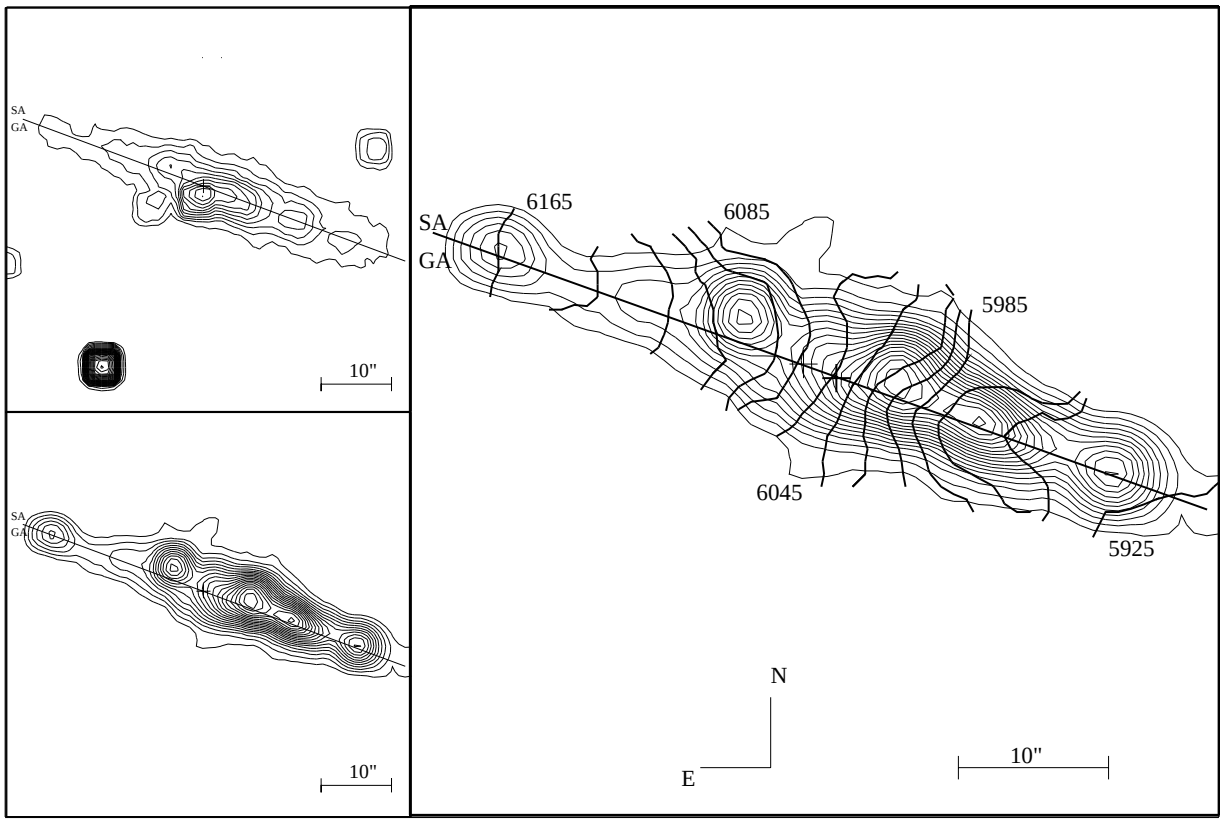

Fig. 5a.— HCG 88d: same as Fig.1a

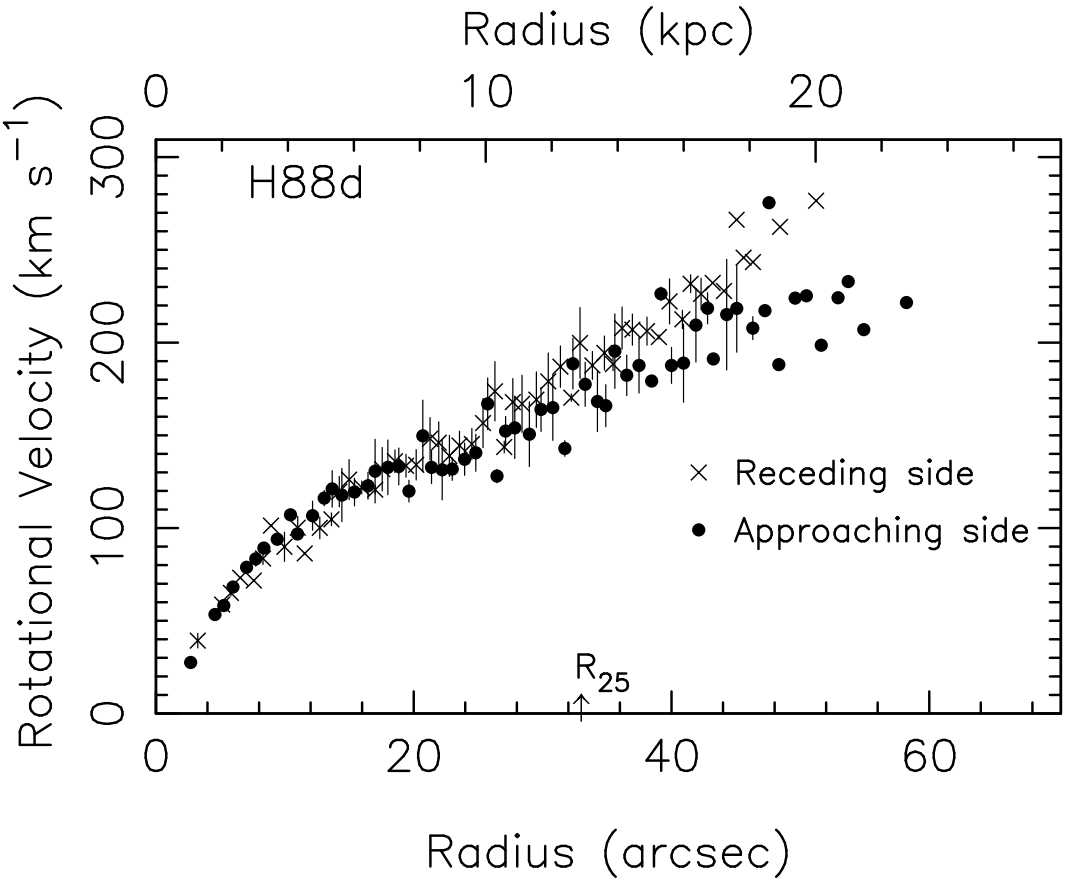

Fig. 5b.— HCG 88d: same as Fig.1b

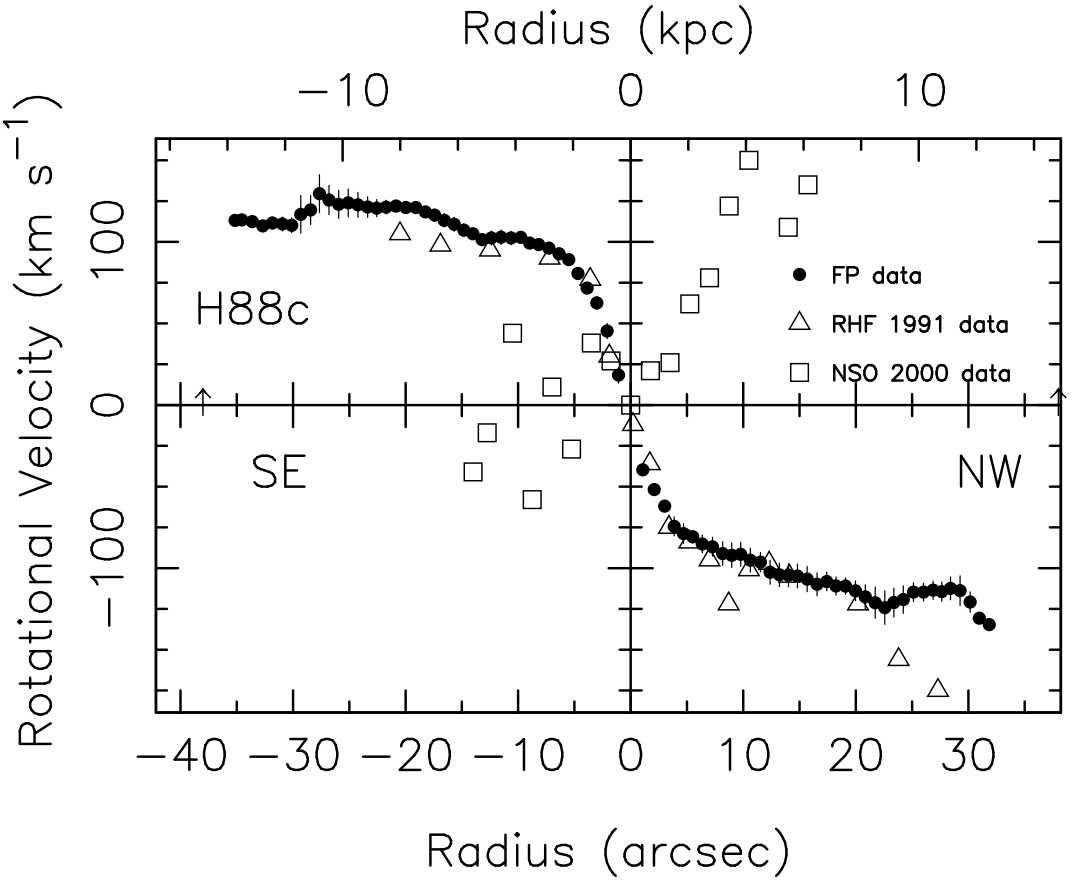

Fig. 6a.— HCG 88c: we are presenting different rotation curves using our data, RFH1991 data and NSOMT2000 data. The kinematical parameters used to plot the rotation curves are, for the inclination, 42^o, 34^o and 32^o respectively and for the position angle of the major axis, 150^o, 160^o and 31^o respectively.

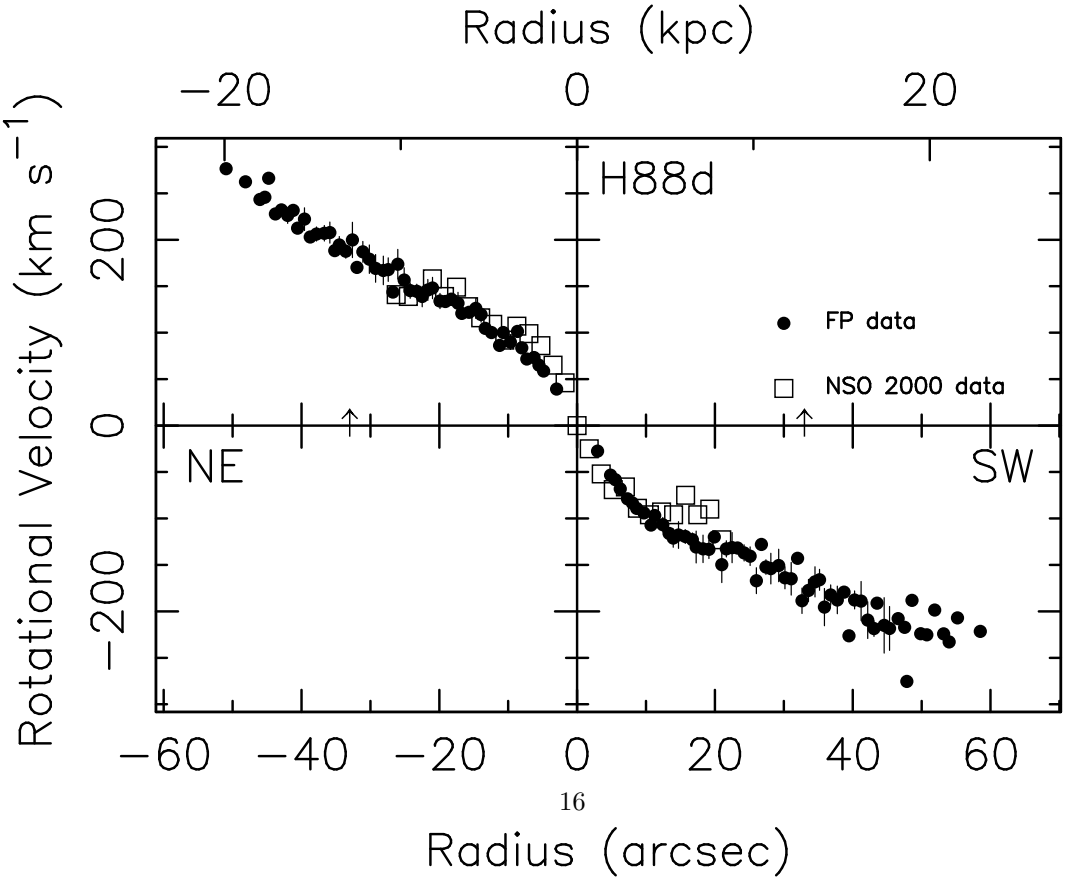

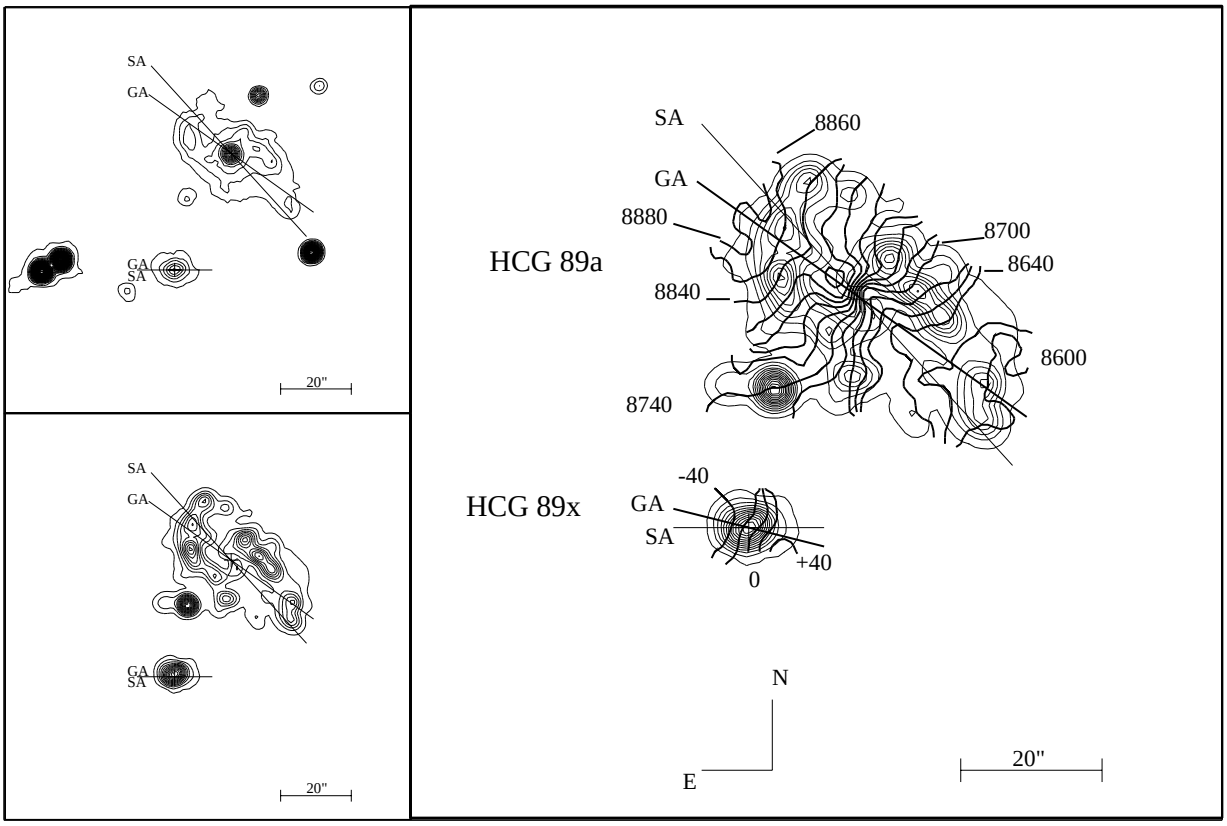

Fig. 7a.— HCG 89a: same as Fig. 1a. Monochromatic and velocity maps for HCG 89x are presented

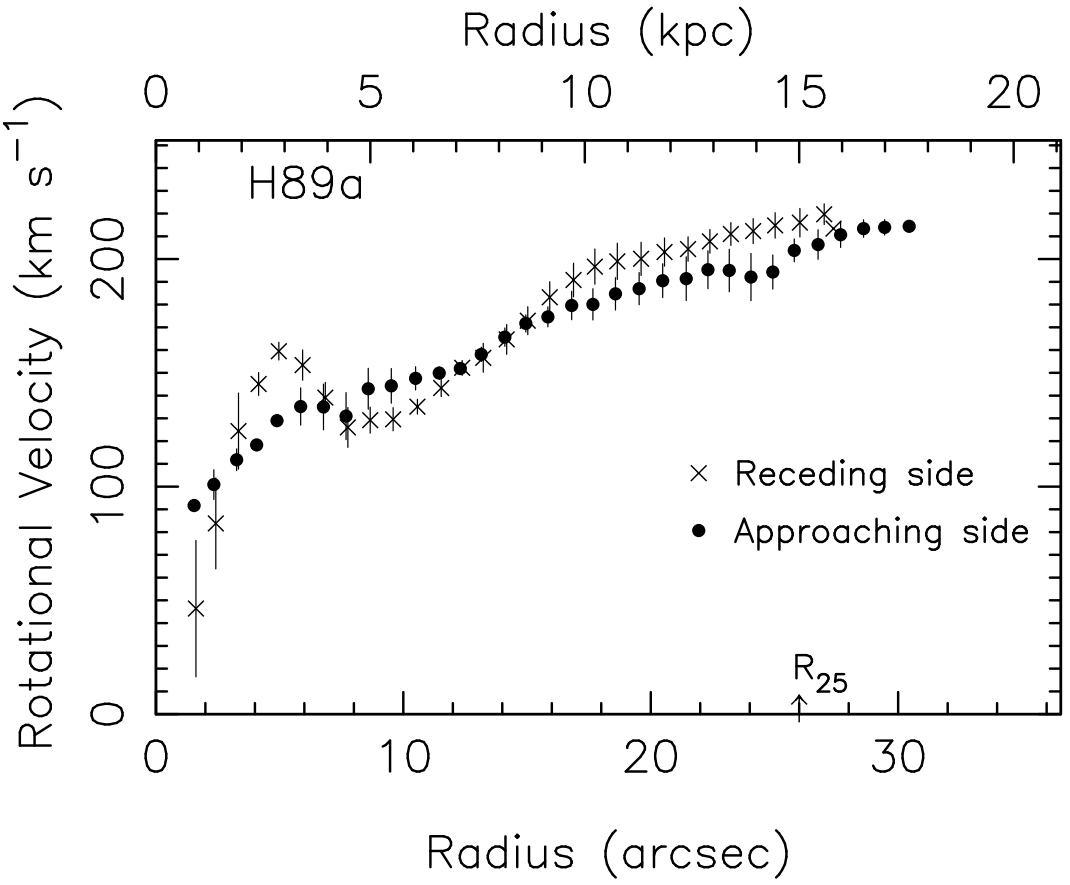

Fig. 7b.— HCG 89a: same as Fig.1b

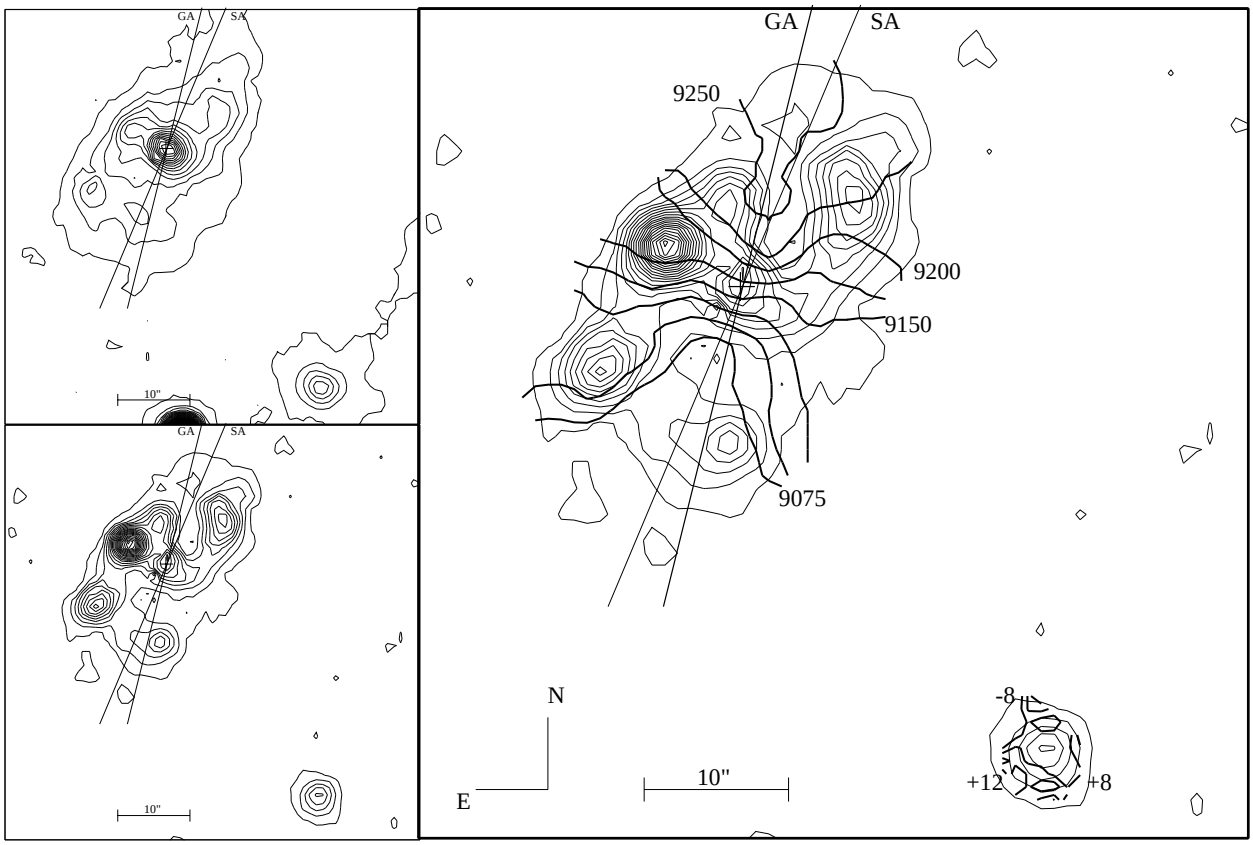

Fig. 8a.— HCG 89b: same as Fig. 1a. Monochromatic and velocity maps for an object on the south west of the field are presented.

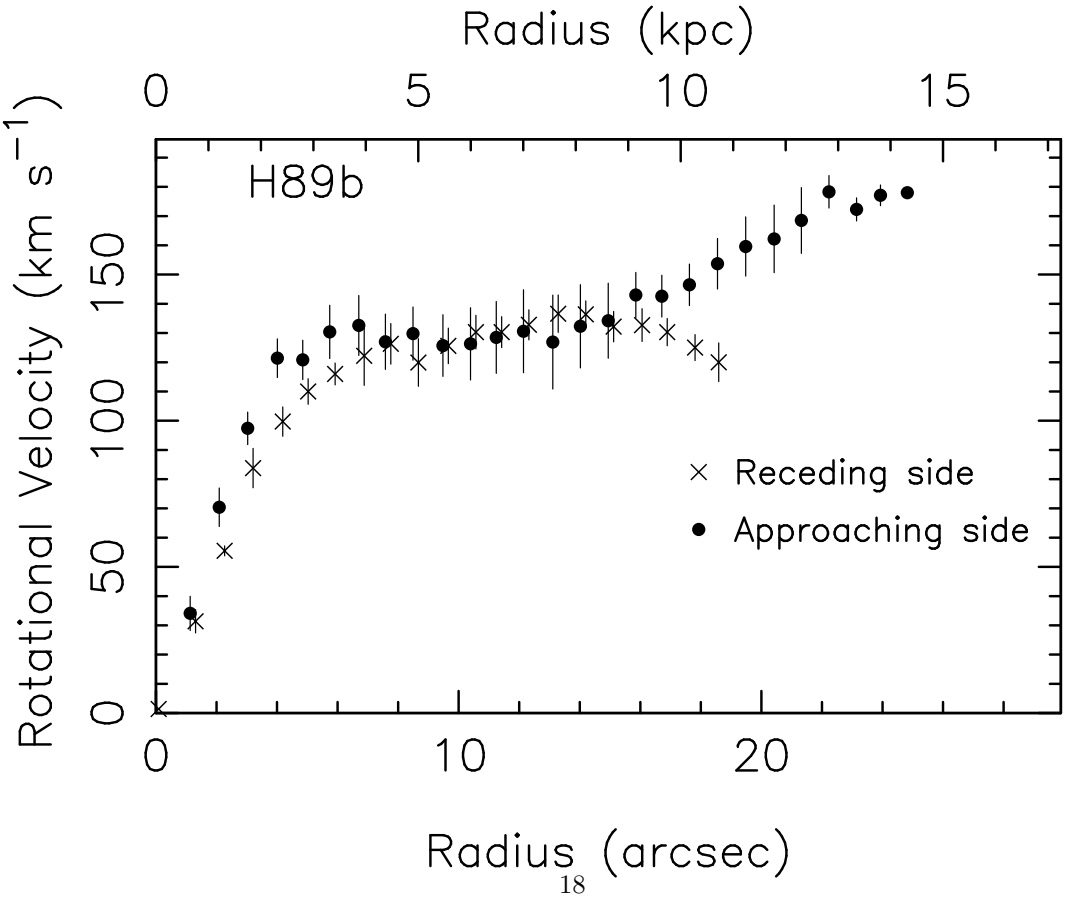

Fig. 8b.— HCG 89b: same as Fig.1b

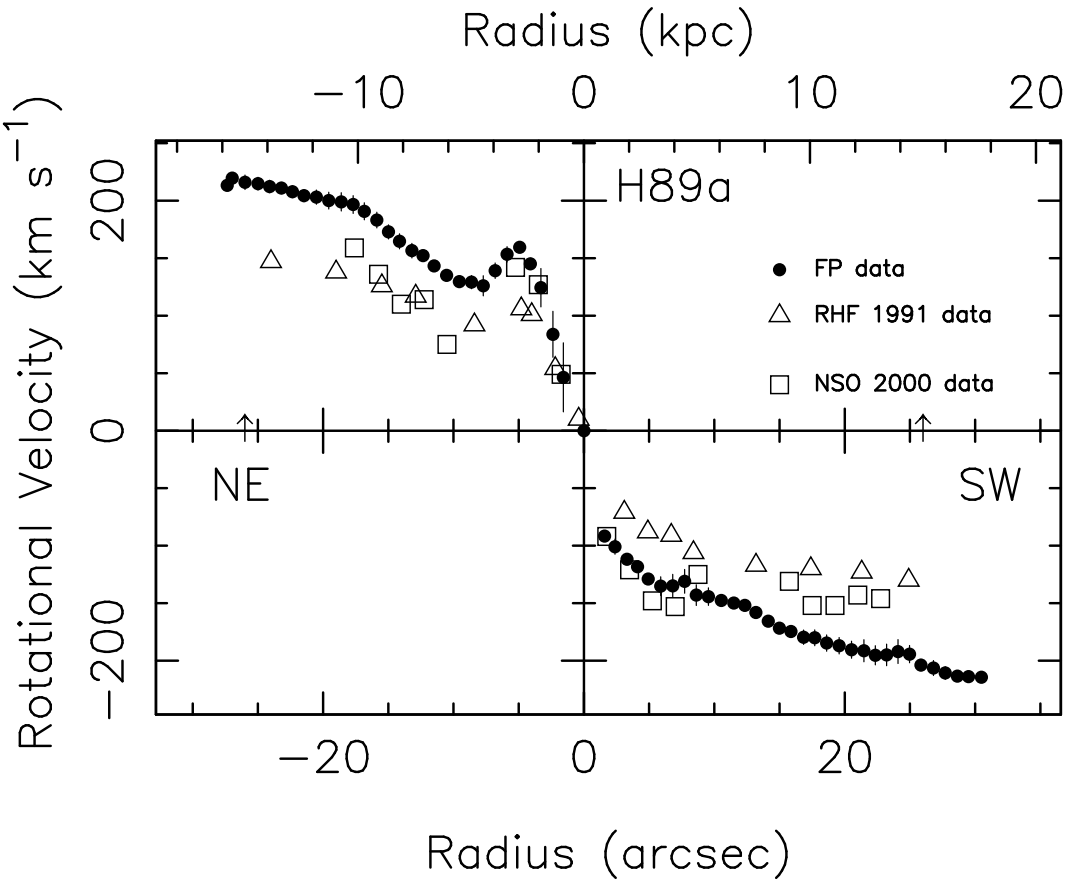

Fig. 9a.— HCG 89a: we are presenting different rotation curves using our data, RHF1991 data and NSOMT2000 data. The kinematical parameters used to plot the rotation curves are, for the inclination, 45^o, 60^o and 51^o respectively and for the position angle of the major axis, 54^o, 52^o and 57^o respectively.

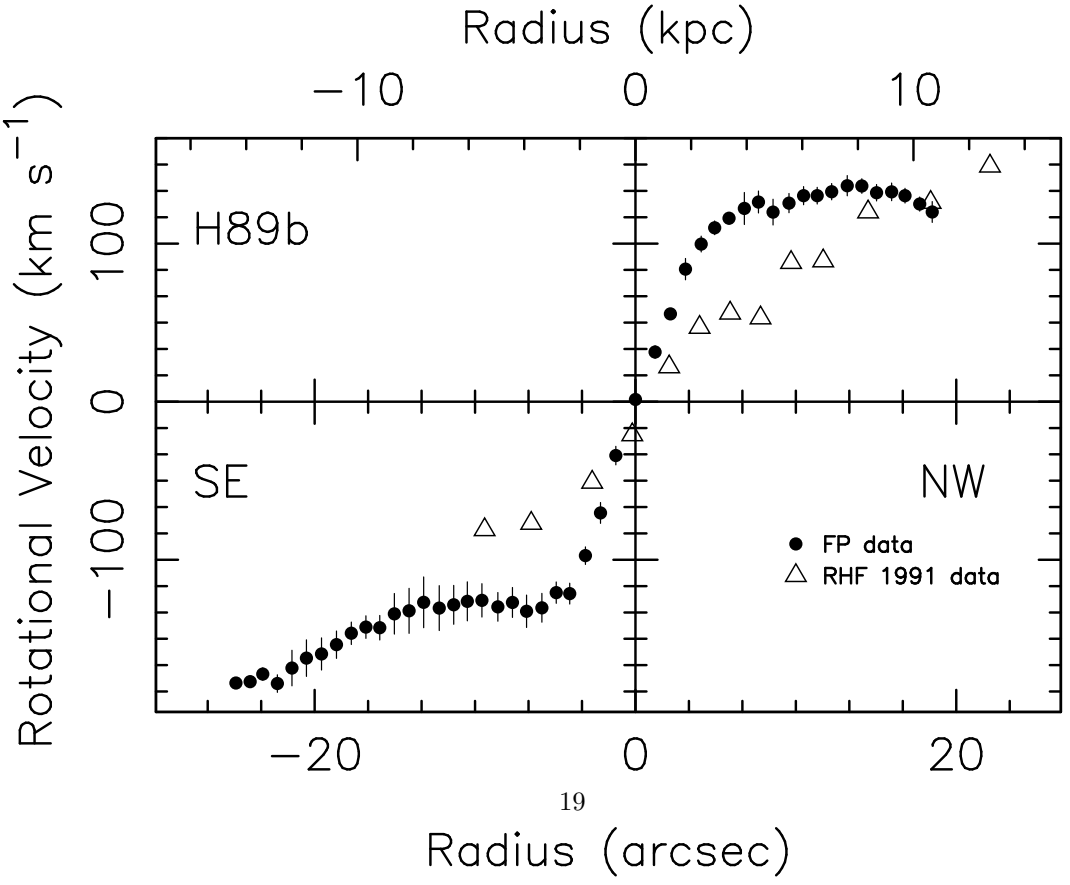

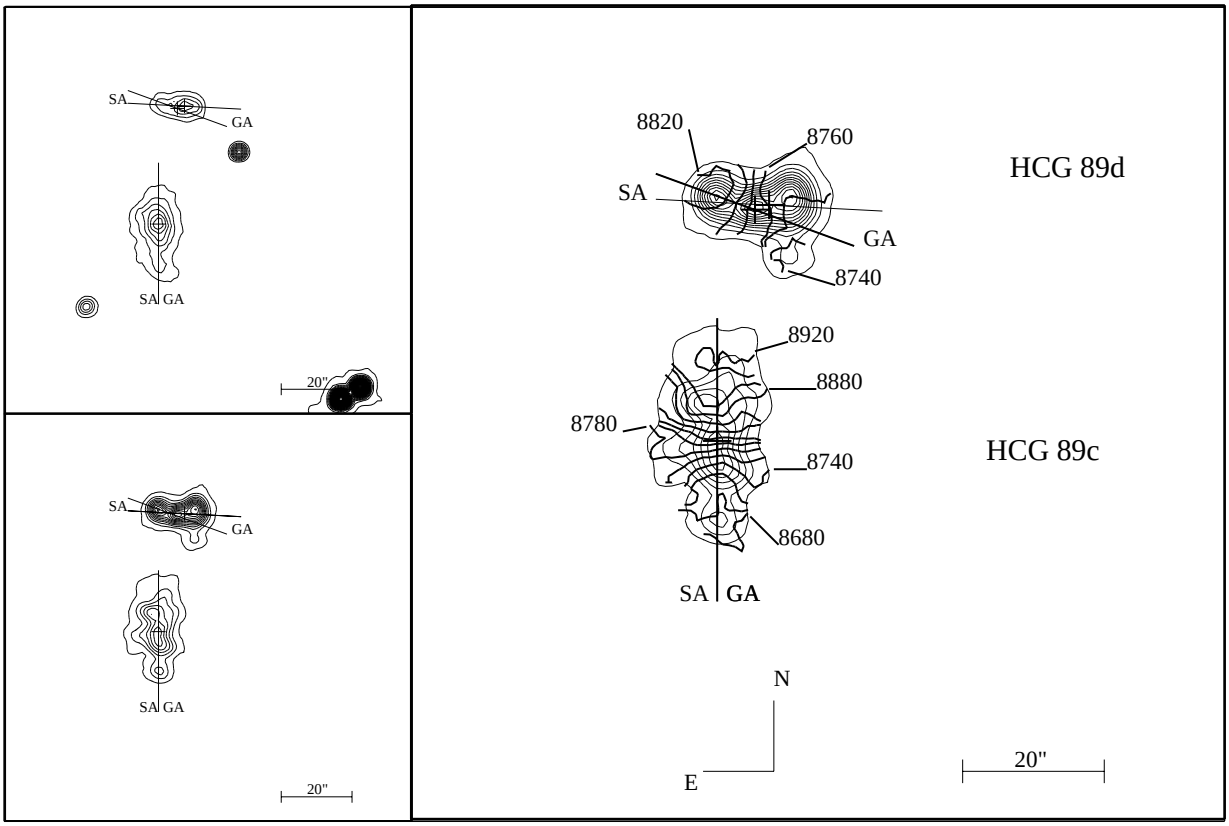

Fig. 10a.— HCG 89c-d: same as Fig.1a

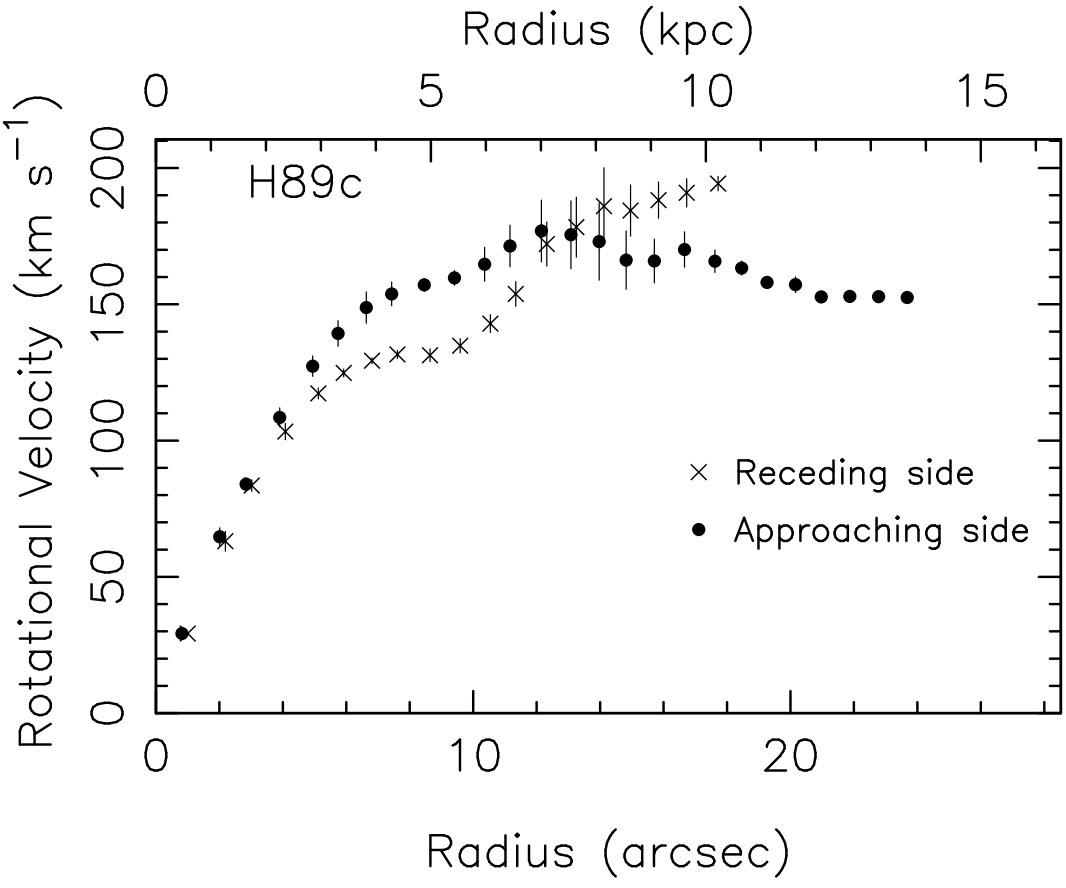

Fig. 10b.— HCG 89c: same as Fig.1b

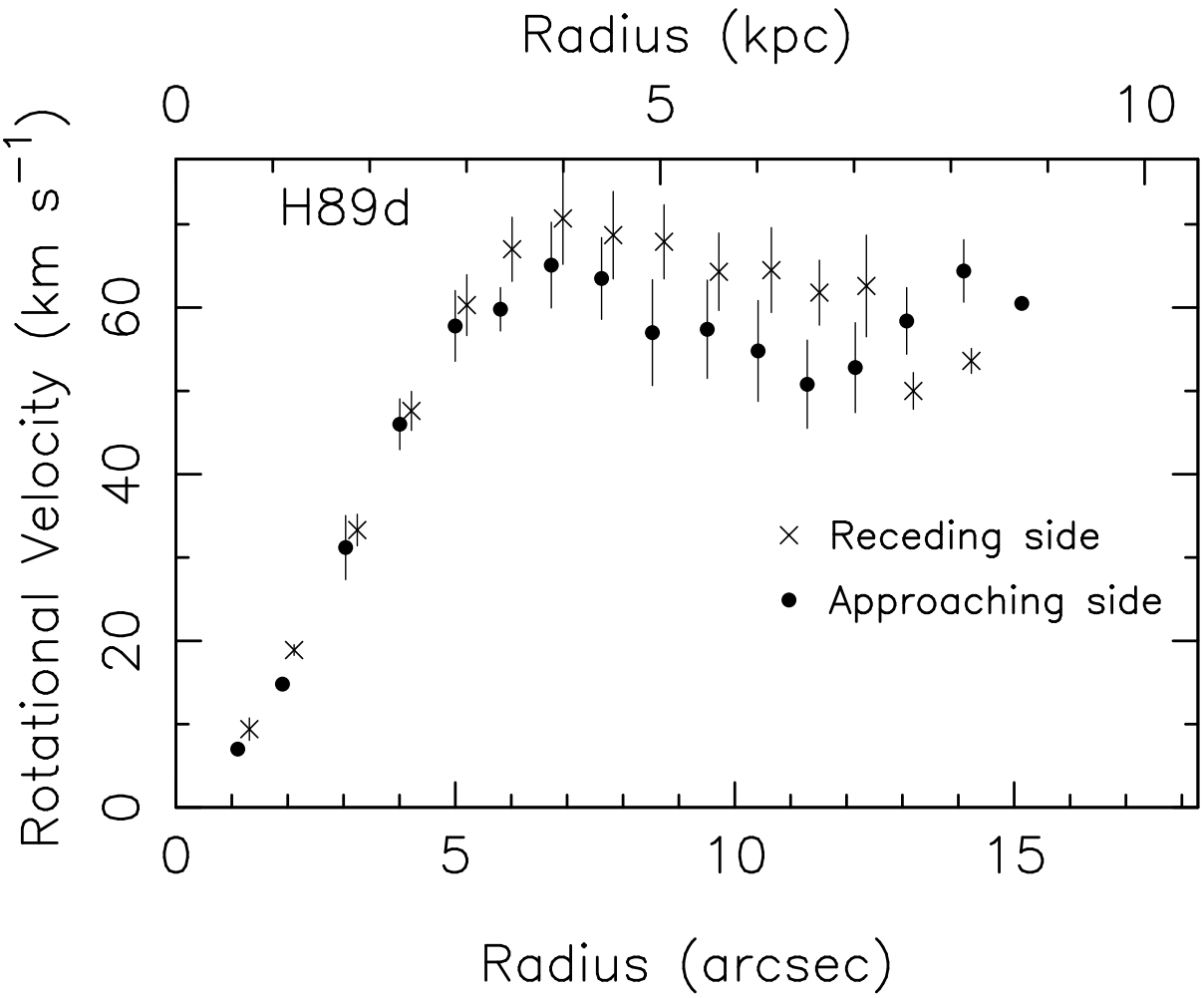

Fig. 11a.— HCG 89d: same as Fig.1b

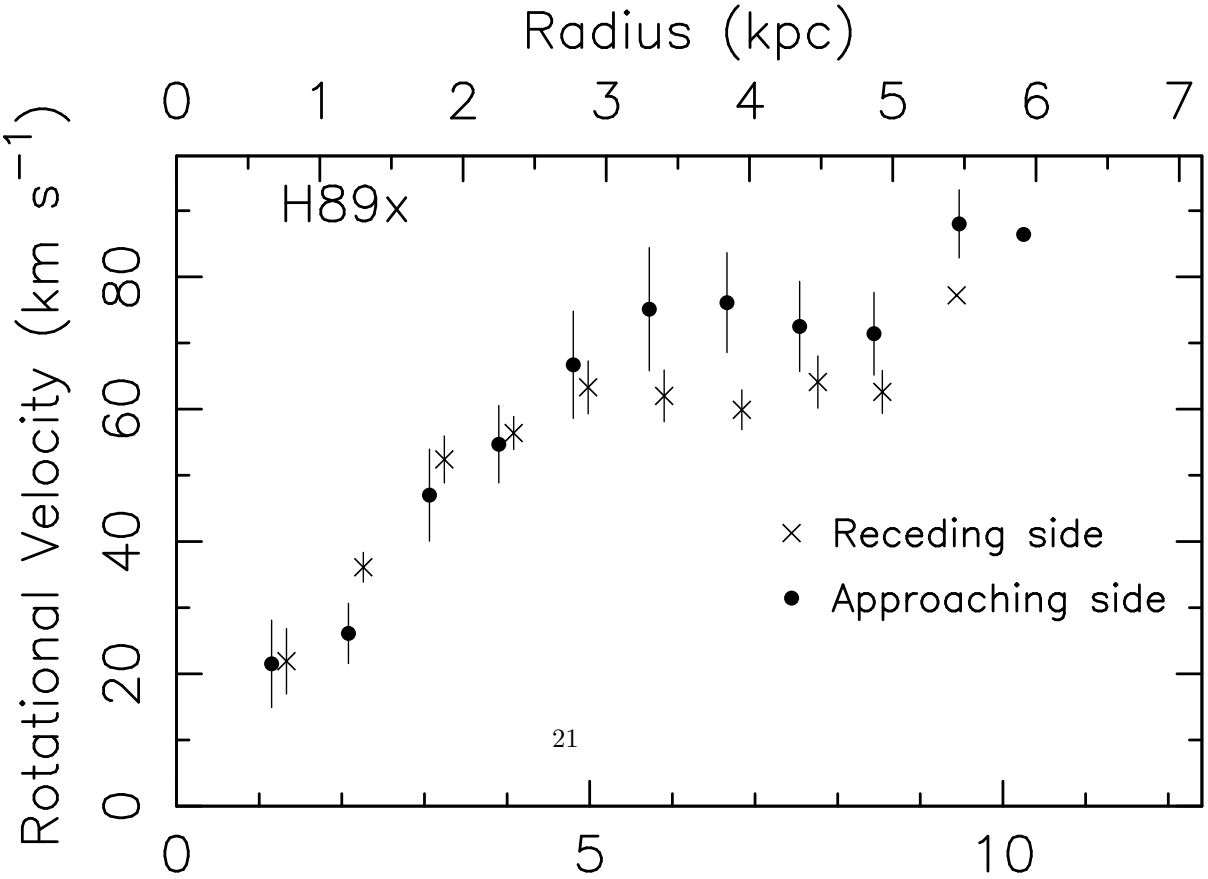

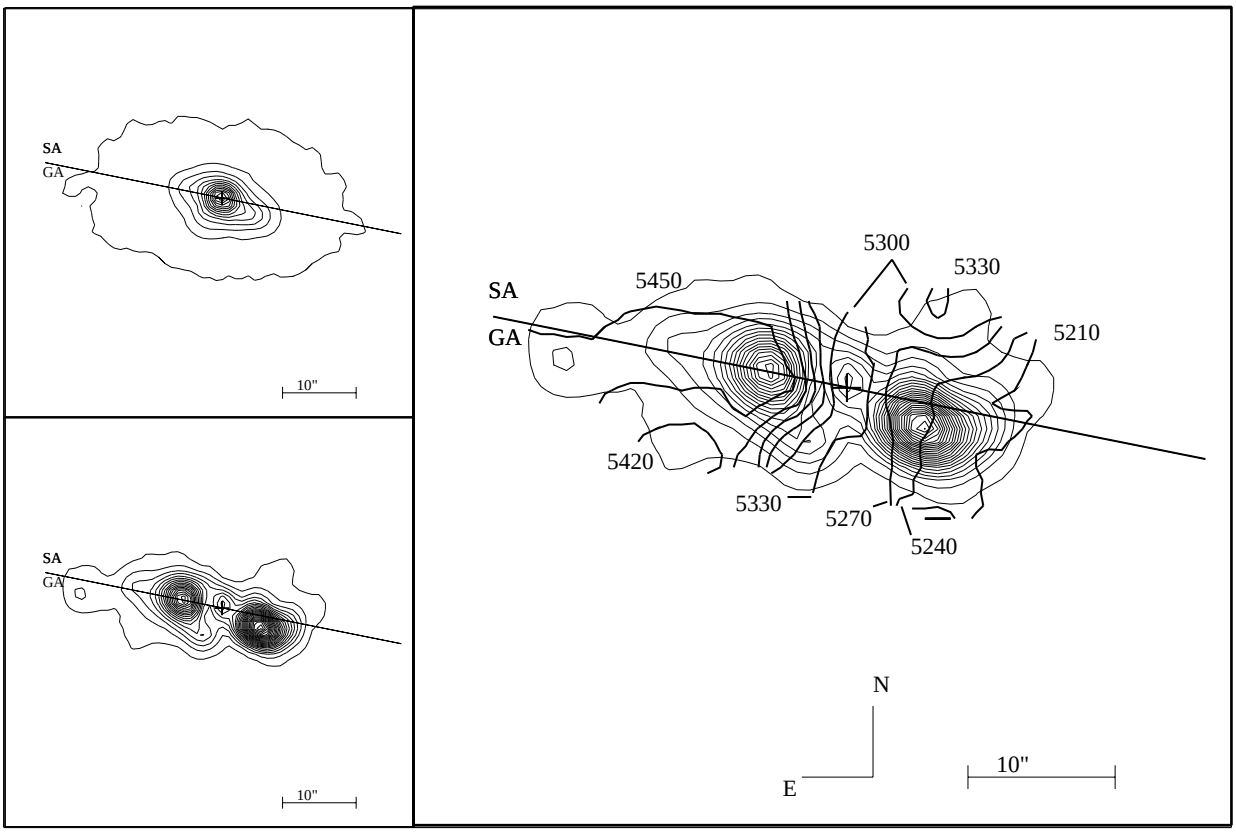

Fig. 12a.— HCG 100a: same as Fig.1a

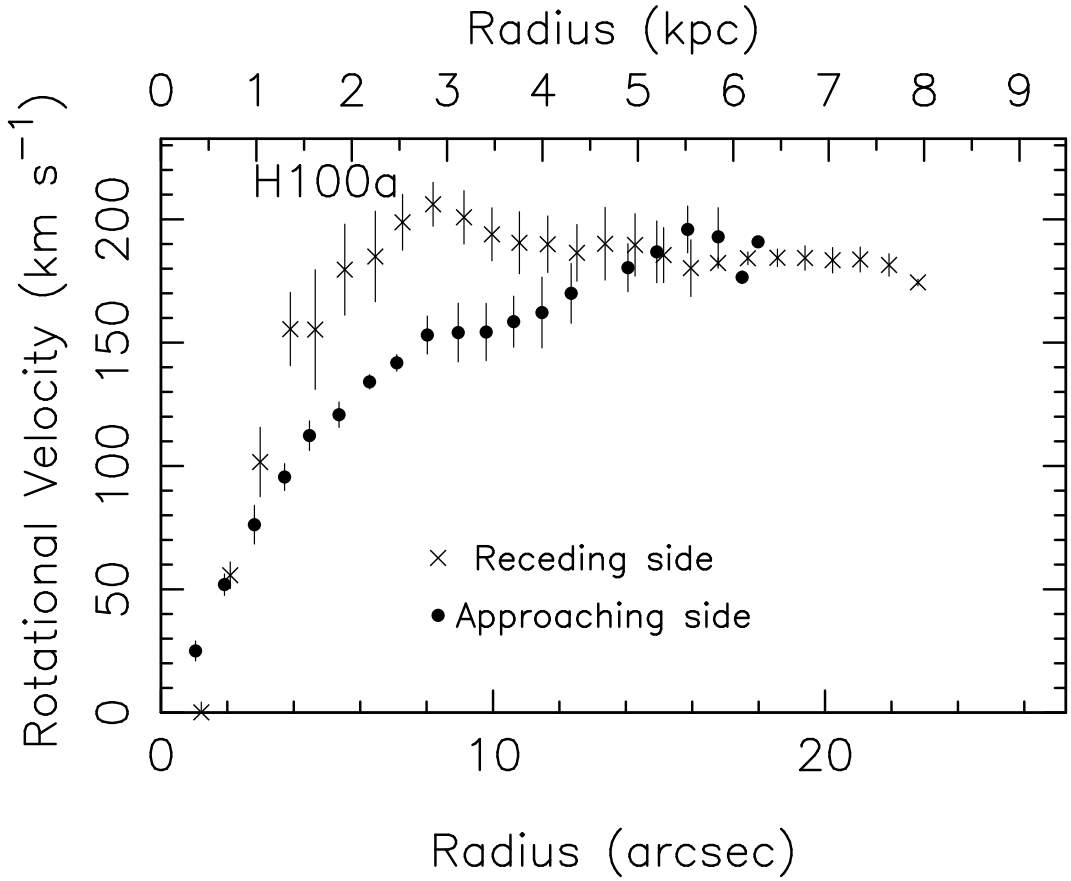

Fig. 12b.— HCG 100a: same as Fig.1b

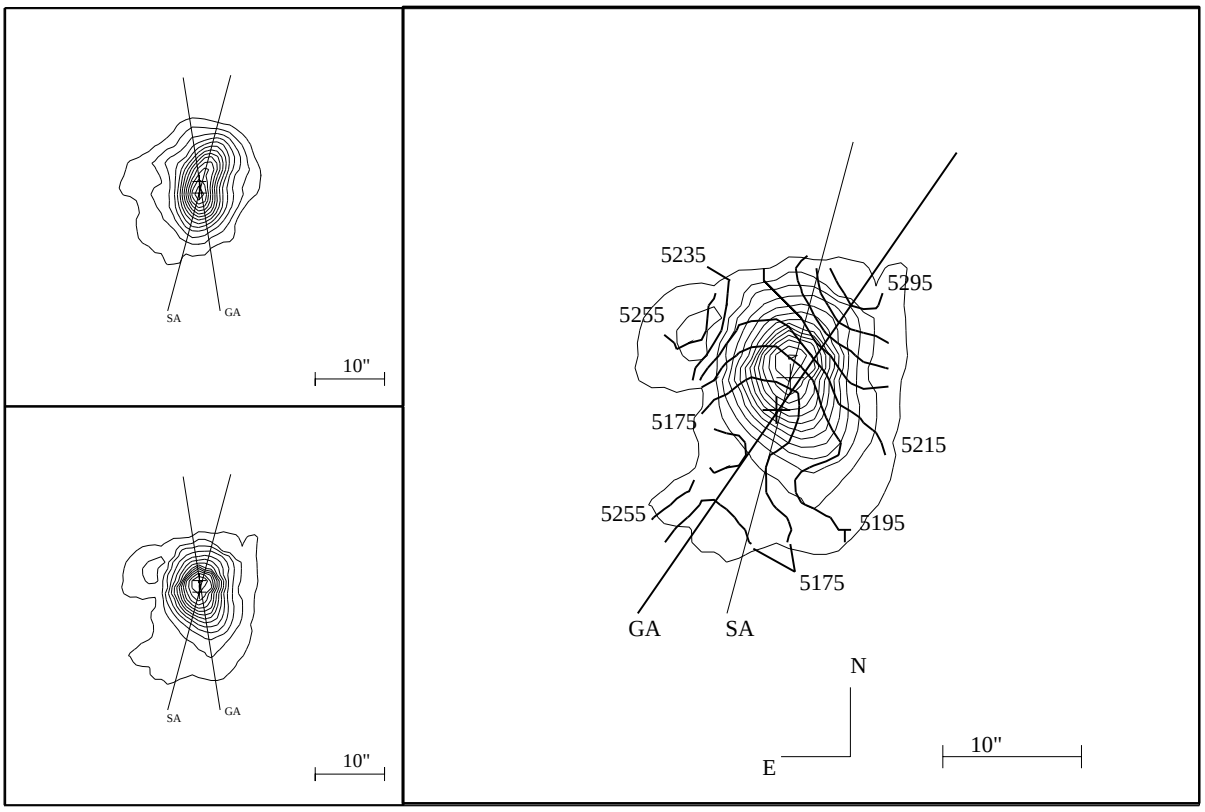

Fig. 13a.— HCG 100b: same as Fig.1a

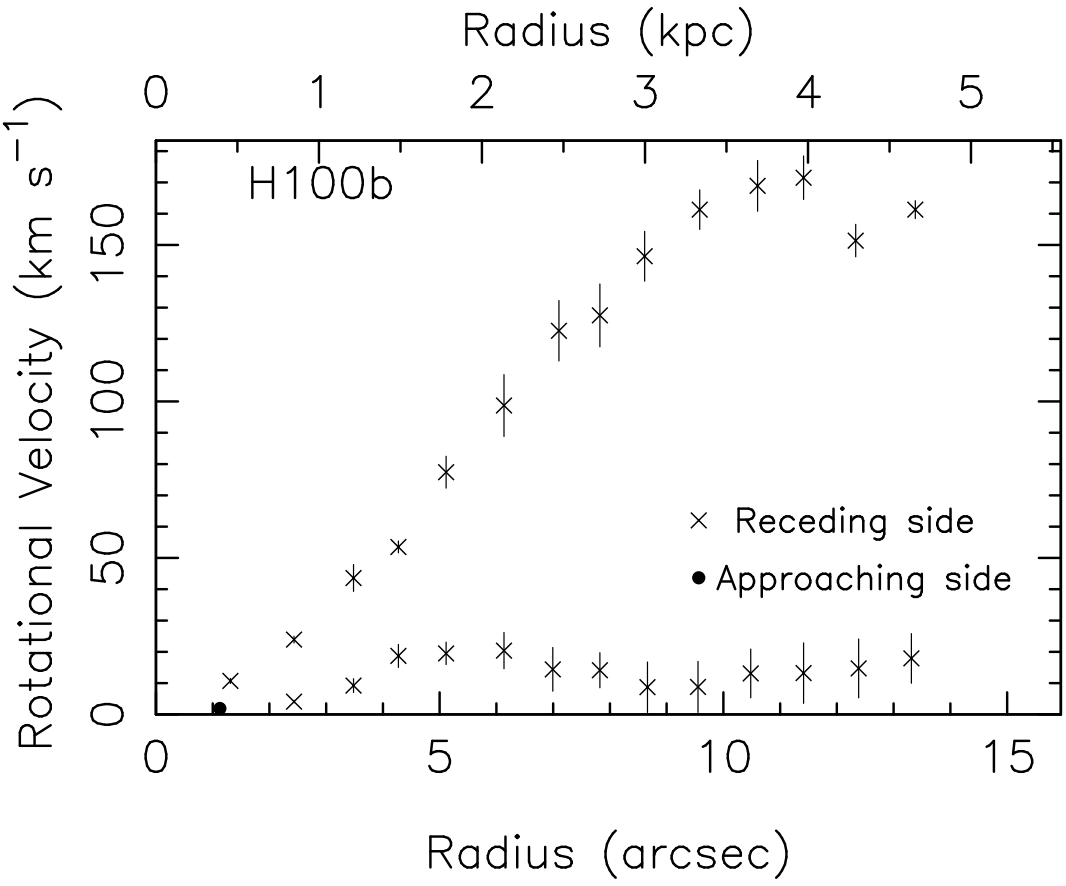

Fig. 13b.— HCG 100b: same as Fig.1b

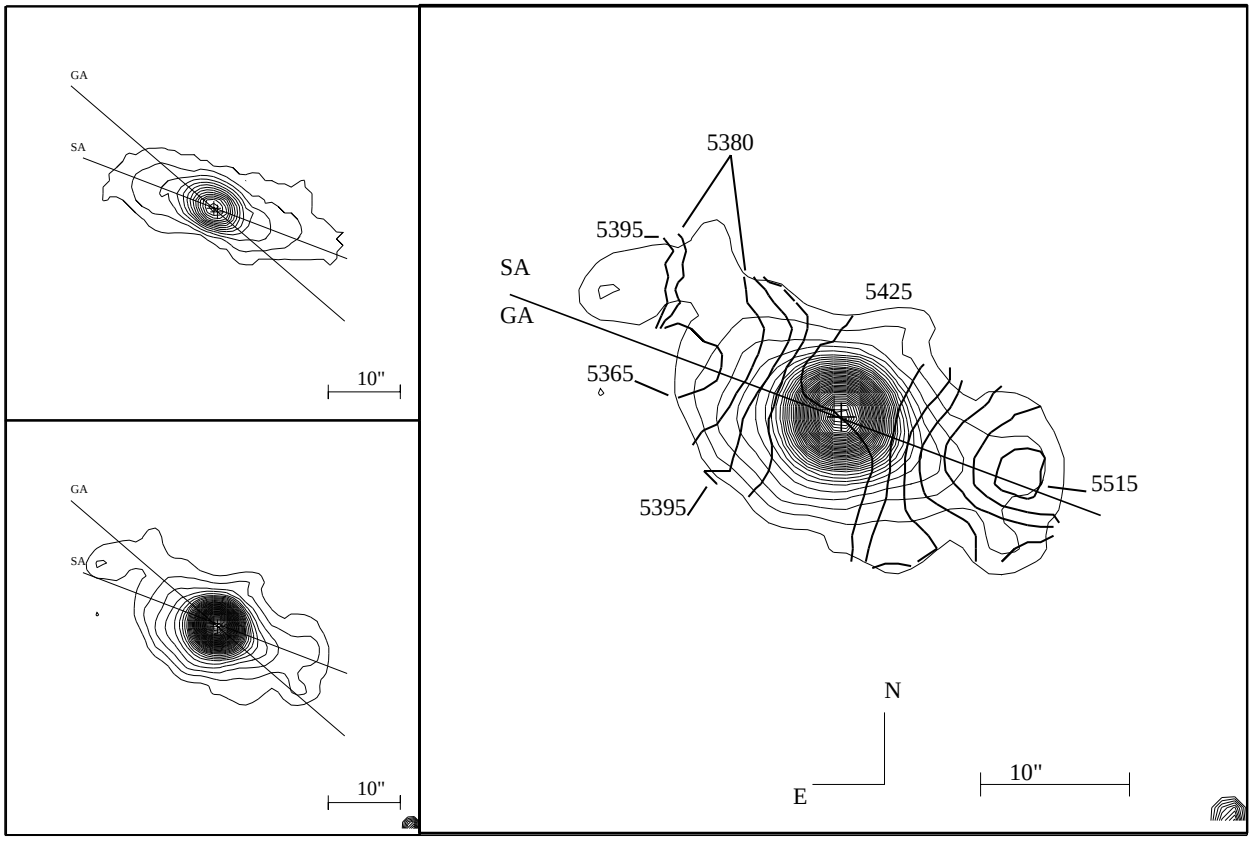

Fig. 14a.— HCG 100c: same as Fig.1a

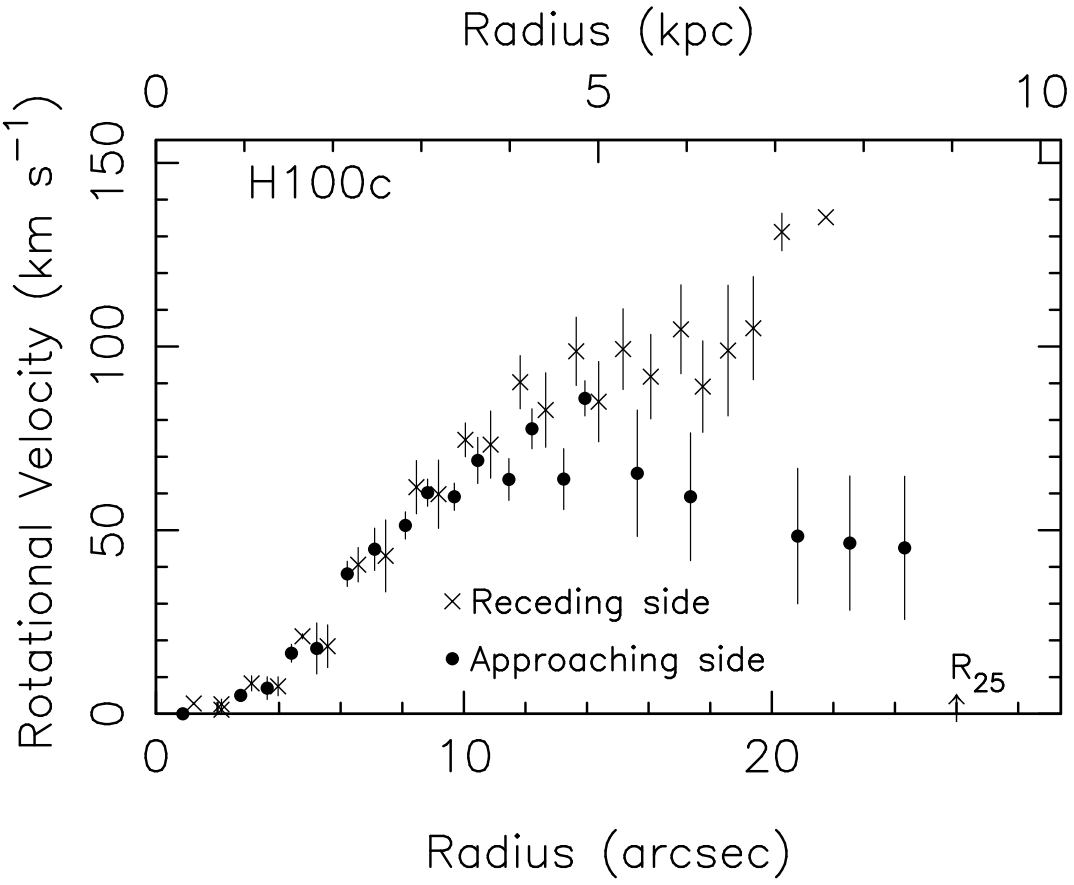

Fig. 14b.— HCG 100c: same as Fig.1b

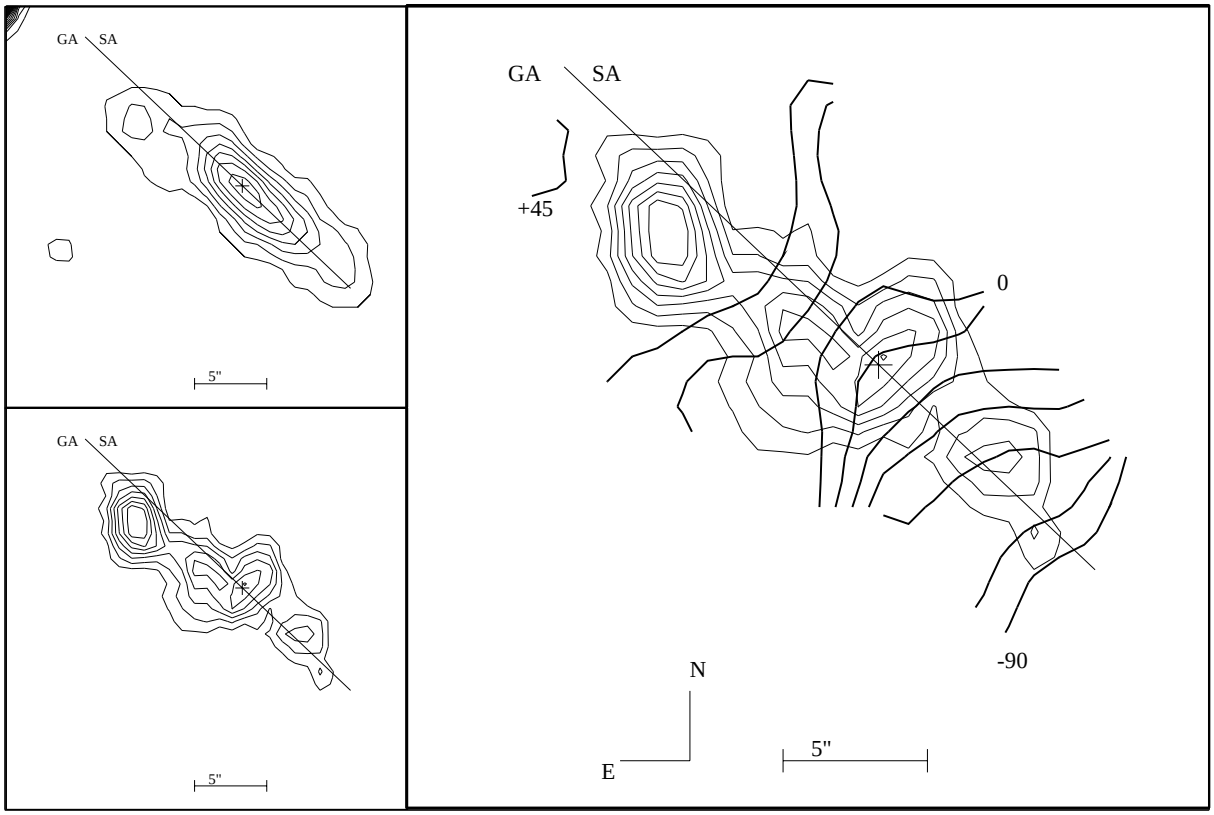

Fig. 15a.— HCG 100d: same as Fig.1a

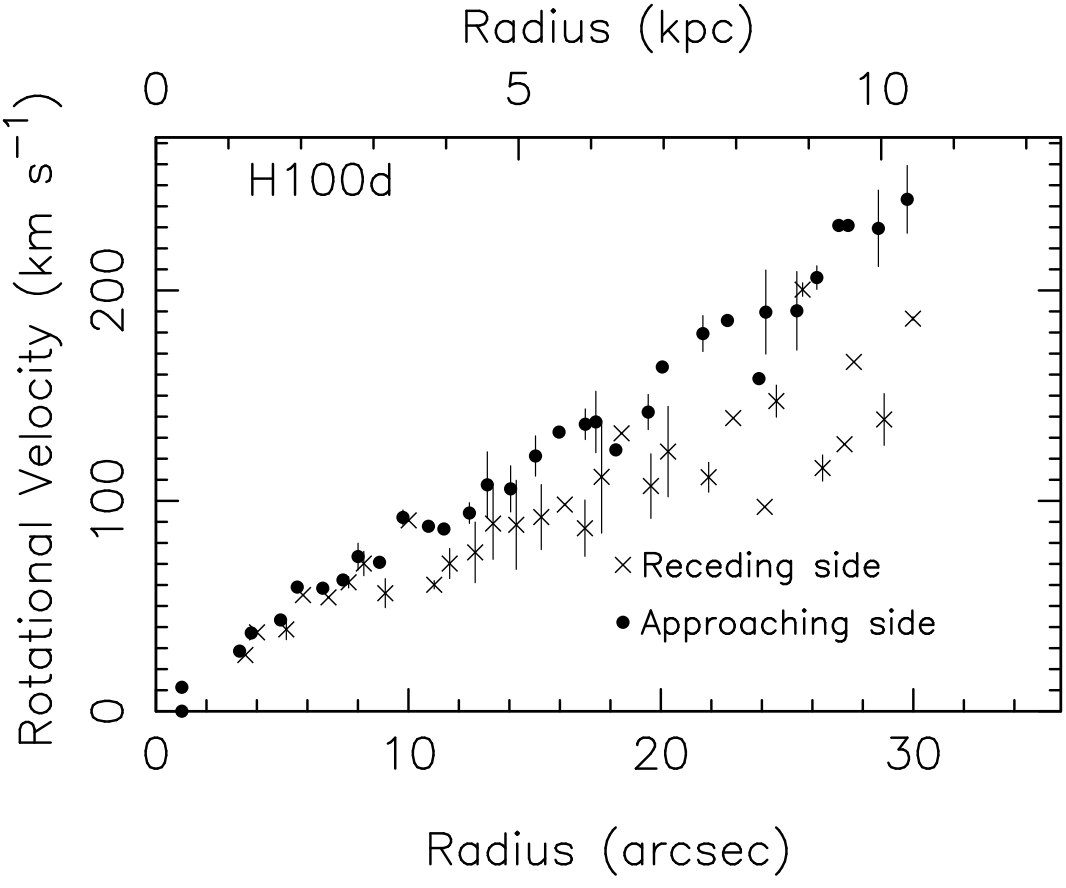

Fig. 15b.— HCG 100d: same as Fig.1b

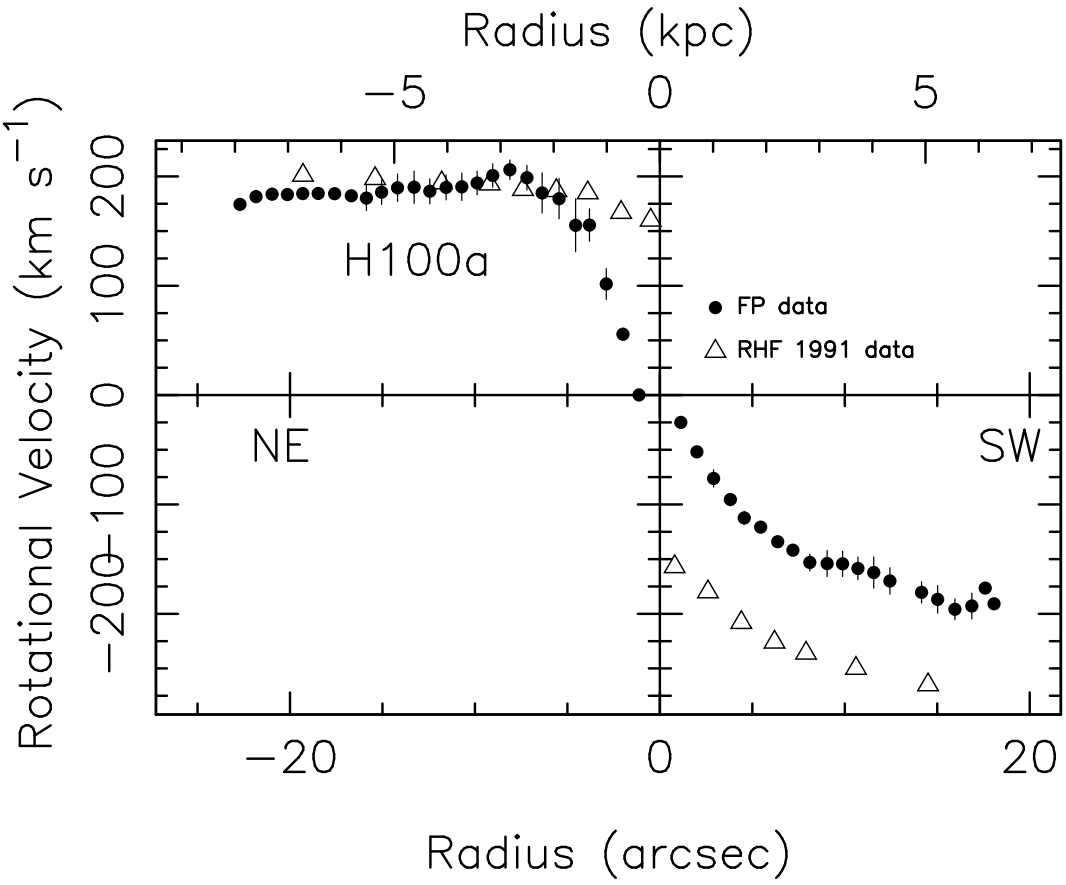

Fig. 16a.— HCG 100a: we are presenting different rotation curves using our data and RFH1991 data. The kinematical parameters used to plot the rotation curves are, for the inclination, 50^o and 60^o respectively and for the position angle of the major axis, 78^o and 85^o respectively.

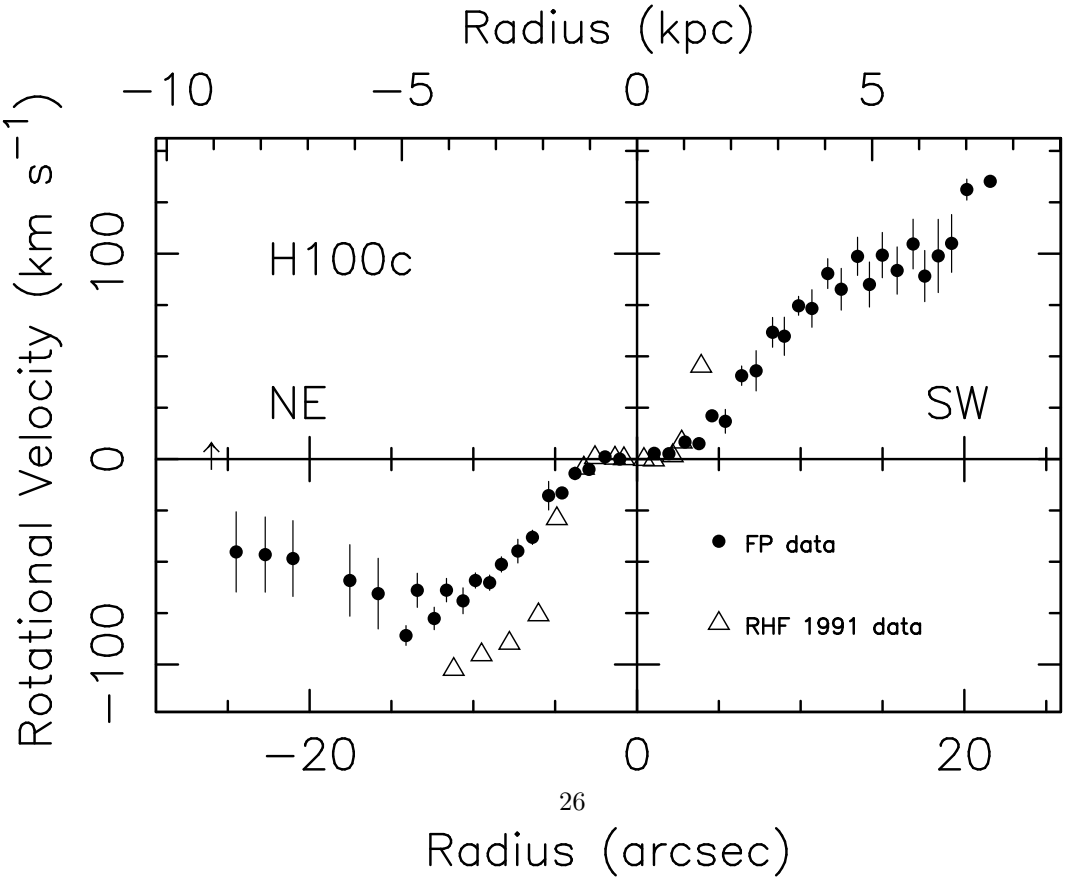

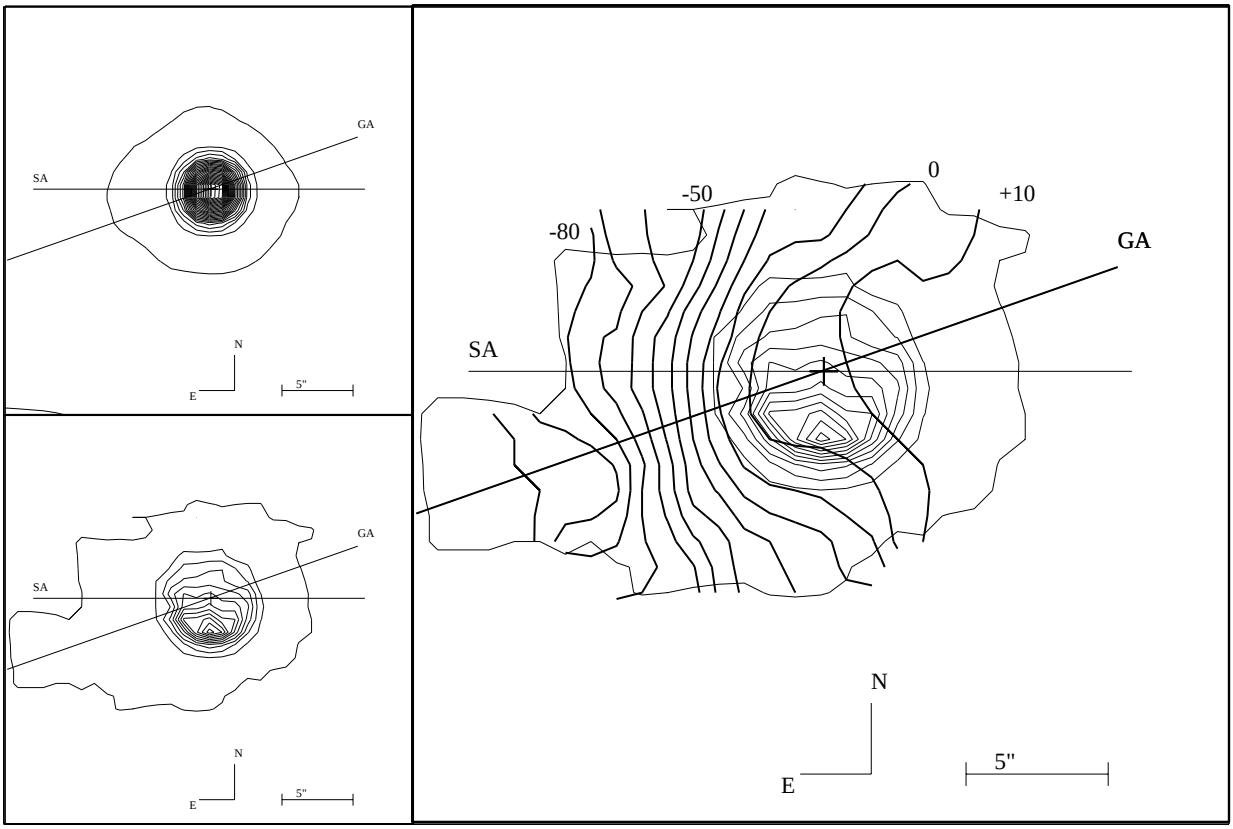

Fig. 17a.— HCG 100x: same as Fig.1a

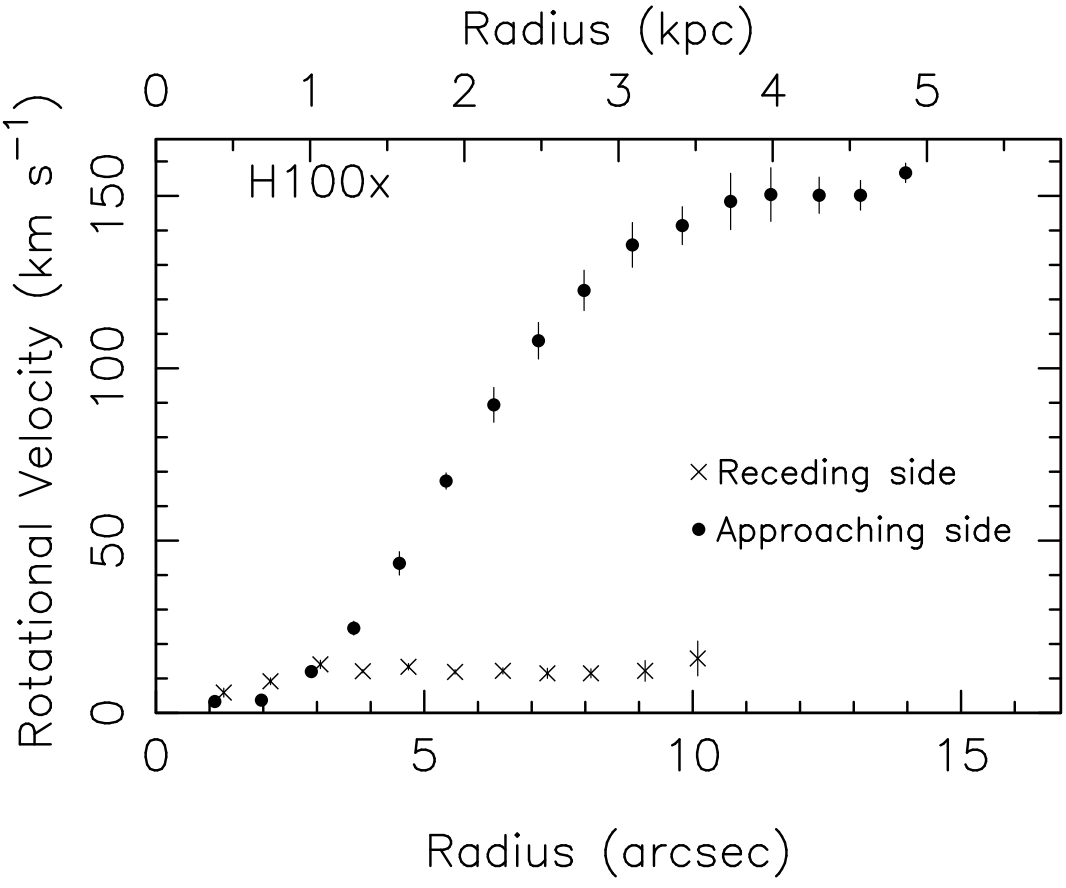

Fig. 17b.— HCG 100x: same as Fig.1b

TABLE 1
JOURNAL OF PEROT-FABRY OBSERVATIONS

	Hickson Compact Groups		
Observations	Telescope	CFHT 3.6m	ESO 3.6m
	Equipment	MOS/FP @ Cassegrain	CIGALE @ Cassegrain
	Date	1996, August, 27-29	1995, August, 21-24
	Seeing	< 1"	~ 1"
Calibration	Neon Comparison light	λ 6598.95 Å	λ 6598.95 Å
Perot–Fabry	Interference Order	1162 @ 6562.78 Å	796 @ 6562.78 Å
	Free Spectral Range at Hα	265 $km\ s^{-1}$	380 $km\ s^{-1}$
	Finesse at Hα	12	12
	Spectral resolution at Hα	13672 [1]	9375 [1]
Sampling	Number of Scanning Steps	24	24
	Sampling Step	0.24 Å (11 $km\ s^{-1}$)	0.35 Å (16 $km\ s^{-1}$)
	Total Field	440"×440" (512×512 px^2)[2]	170"×170" (256×256 px^2)
	Pixel Size (binned)	0.86"	0.91"
Detector		STIS 2 CCD	IPCS

[1]For a signal to noise ratio of 5 at the sample step

[2]After binning 2*2

TABLE 2
OBSERVATIONAL CHARACTERISTICS

Name	Telescope	Exposure Time		Interference Filter		
		Total	per channel	Central wavelength	FWHM	Transmission at maximum
HCG 88 ab	ESO 3.6m	2h	300s	6688 Å	22 Å	0.73
cd	CFHT 3.6m	1.2h	180s	6697 Å	17 Å	0.73
HCG 89	ESO 3.6m	2h	300s	6763 Å	30 Å	0.73
HCG 100acd	CFHT 3.6m	1.2h	180s	6697 Å	17 Å	0.73
b	ESO 3.6m	2h	300s	6668 Å	20 Å	0.60

TABLE 3
PROPERTIES OF HCGS MEMBERS

Name	α (1950)	δ (1950)	Morphological[1] Type	Systemic[1] Velocity ($km\ s^{-1}$)	B_{TC}[1]	R_{25}[2] (Arcsec)
HCG 88 a	20h 49m 55.6s	-05°53′59.7″	Sb	6033	13.18	44
b	20h 49m 51.0s	-05°56′08.5″	SBb	6010	13.24	37
c	20h 49m 47.2s	-05°57′40.8″	Sc	6083	13.87	38
d	20h 49m 33.9s	-05°59′12.7″	Sc	6032	14.49	33
HCG 89 a	21h 17m 24.3s	-04°08′04.4″	Sc	8850	14.10	26
b	21h 17m 42.5s	-04°06′31.8″	SBc	8985	14.88	-
c	21h 17m 31.6s	-04°07′48.7″	Scd	8872	15.52	-
d	21h 17m 31.2s	-04°07′14.6″	Sm	8857	16.27	-
HCG 100 a	23h 58m 46.3s	+12°49′57.2″	Sb	5300	13.66	30
b	23h 58m 52.4s	+12°50′03.8″	Sm	5253	14.90	23
c	23h 58m 39.8s	+12°51′56.1″	SBc	5461	15.22	26
d	23h 58m 41.0s	+12°50′03.3″	Scd	-	15.97	-

[1]Optical systemic velocities from Hickson 1993

[2]From NED

TABLE 4
KINEMATICAL PROPERTIES OF THE HCGS

Name	Position Angle (in degree)			Inclination (in degrees)			Rotation velocity	Systemic velocity [1]
	Velocity map	Cont. map	Mono. map	Velocity map	Cont. map	Mono. map	Approaching / Receding side velocity ($km\ s^{-1}$)	$km\ s^{-1}$
HCG 88 a	128 ±5	126 ±10	120 ±10	65 ±5	55 ±3	67 ±5	-280 / +300	5963
b	160 ±5	34 ±10	-	55 ±3	45 ±?	-	-260 / +265	6024
c	150 ±3	-	-	42 ±2	-	-	-121 / +130	5979
d	70 ±5	70 ±8	70 ± 8	85 ±2	73 ±3	73 ±5	-200 / +220	6037
HCG 89 a	54 ±6	44 ±10	44 ±10	45 ±5	51 ±3	51 ±5	-214 / +220	8736
b	165 ±5	155 ±10		49±3	65±3	-	-165 / +130	8778
c	0 ±3	0 ±3	0 ±5	46 ±3	65 ±3	65 ±5	-165 / +190	8799
d	70 ±7	87 ±7	85 ±8	50 ±5	45 ±3	45 ±5	-55 / +65	8775
x	80 ±3	90 ±3	90 ±3	50 ±3	30 ±3	30 ±5	-78 / +62	-
HCG 100 a	78 ±5	78 ±5	78 ±10	50 ±7	47 ±3	59 ±5	-190 / +190	5323
b	145 ±5	165 ±5	10 ±5	52 ±10	57 ±3	55 ±5	+13 / +170	5163
c	72 ±8	70 ±5	50 ±5	66 ±5	65 ±3	48 ±5	-70 / +100	5418
d	53 ±3	47 ±5	45 ±5	85 ±5	64 ±3	64 ±5	-170 / +240	-
x	100 ±8	90 ±8	100 ±8	50 ±10	44±10	38±10	-150 / +10	

[1] in $km\ s^{-1}$, from our velocity field and rotation curve

TABLE 5
INTERACTION INDICATORS

Indicators	H88a	HGC 88b	HGC 88c	HGC 88d
Highly disturbed velocity field	-	+	-	-
Central double nuclei	-	-	-	-
Double kinematic gas component	-	-	-	-
Changing PA along major axis	-	+	-	-
Gaseous versus stellar major-axis misalignment	-	+	-	-
Tidal tails	-	-	-	-
High IR luminosity	+	+	-	-
Central activity	+	+	-	-
	HGC 89a	HGC 89b	HGC 89c	HGC 89d
Highly disturbed velocity field	+	+	+	+
Central double nuclei	-	-	-	-
Double kinematic gas component	-	-	-	-
Changing PA along major axis	+	+	-	+
Gaseous versus stellar major-axis misalignment	+	+	-	+
Tidal tails	-	+	-	-
High IR luminosity	-	-	-	-
Central activity	-	-	-	-
	HGC 100a	HGC 100b	HGC 100c	HGC 100d
Highly disturbed velocity field	+	+	+	+
Central double nuclei	-	+	-	-
Double kinematic gas component	-	-	-	-
Changing PA along major axis	+	+	+	-
Gaseous versus stellar major-axis misalignment	-	+	+	-
Tidal tails	-	+	-	-
High IR luminosity	+	-	-	-
Central activity	-	-	-	-